An inosine triphosphate pyrophosphatase safeguards nucleic acids from aberrant purine nucleotides and prevents a constitutive salicylic acid response

Henryk Straube[1], Jannis Straube[2], Jannis Rinne[1], Markus Niehaus[1], Hanna Rose[3], Claus-Peter Witte[1] and Marco Herde*[1]

[1] Department of Molecular Nutrition and Biochemistry of Plants, Leibniz Universität Hannover, Hannover, 30419, Germany
[2] Department of Molecular Plant Breeding, Leibniz Universität Hannover, Hannover, 30419, Germany
[3] Department of Phytomedicine, Leibniz Universität Hannover, Hannover, 30419, Germany

* Address correspondence to: mherde@pflern.uni-hannover.de

Short title: ITPA removes deaminated purine nucleotides.

One-sentence summary: ITPA dephosphorylates deaminated purine nucleotides that arise from oxidative stress and thus contributes to nucleic acid integrity.

ABSTRACT

Inosine is deaminated adenosine. Inosine is enzymatically introduced in some plant tRNAs but not in other RNAs or DNA. Nonetheless, our data show that RNA and DNA from *Arabidopsis thaliana* contain (deoxy)inosine, probably derived from non-enzymatic adenosine deamination in nucleic acids and usage of (deoxy)inosine triphosphate (ITP / dITP) during nucleic acid synthesis. We identified a plant INOSINE TRIPHOSPHATE PYROPHOSPHATASE (ITPA) which is conserved in many organisms. Arabidopsis ITPA dephosphorylates deaminated nucleoside di- and triphosphates to the respective monophosphates. *ITPA* mutation causes inosine di- and triphosphate accumulation *in vivo* and an elevated (deoxy)inosine content in DNA and RNA. Cadmium-induced oxidative stress, known to foster deamination, leads to more ITP in the wildtype and especially in *itpa* mutants suggesting that ITP originates from ATP deamination. By contrast, erroneous IMP phosphorylation by AMP kinases seems not to be a major ITP source *in vivo* although these enzymes phosphorylate IMP *in vitro*. Mutation of ITPA causes salicylic acid (SA) accumulation, early senescence and upregulation of transcripts associated with immunity and senescence. ITPA is part of a molecular protection system, preventing accumulation of (d)ITP, its usage for nucleic acid synthesis, and probably nucleic acid stress leading to SA accumulation, stress gene induction and early senescence.

INTRODUCTION

Spontaneous or enzymatically catalyzed reactions can lead to damaged or aberrant metabolites (Lerma-Ortiz et al., 2016; Crécy-Lagard et al., 2018; Carole L Linster et al., 2013). In recent years, several advances in the field of damaged plant metabolites have been made (Hanson et al., 2016), like the discovery of enzymes repairing NADH / NADPH hydrates (Niehaus et al., 2014), or removing damaged glutathione (Niehaus et al., 2019) and oxidized deoxyguanosine triphosphate (8-oxo dGTP; (Dobrzanska et al., 2002; Yoshimura et al., 2007). One of the most prominent metabolite classes that are prone to become damaged are nucleotides (Michael Y. Galperin et al., 2006; Nagy et al., 2014; Rudd et al., 2016; Rampazzo et al., 2010). In non-plant organisms, several enzymes have been identified that repair or remove aberrant and often toxic nucleotides, like DEOXYURIDINE TRIPHOSPHATE PYROPHOSPHATASE (DUT1), INOSINE TRIPHOSPHATE PYROPHOSPHATASE (ITPA), 8-OXO DEOXYGUANOSINE TRIPHOSPHATE PYROPHOSPHATASE (8-oxo dGTPase) and multicopy associated filamentation (MAF) family proteins (Nagy et al., 2014). However, little is known about such enzymes in plants. While plant homologues of DUT1 and 8-oxo dGTPase (Dubois et al., 2011; Yoshimura et al., 2007) have been described, a plant ITPA has not been identified.

ITPA enzymes remove deaminated purine nucleotide triphosphates. They hydrolyze the phosphoanhydride bond between the alpha- and betaphosphate of (deoxy)inosine triphosphate (ITP / dITP) probably derived from deamination of (deoxy)adenosine triphosphate (ATP / dATP) or from spurious phosphorylation of inosine monophosphate (IMP). Xanthosine triphosphate (XTP) presumably derived from deamination of guanosine triphosphate (GTP) or spurious phosphorylation of xanthosine monophosphate (XMP) is also a substrate. ITPA generates the corresponding nucleotide monophosphate and pyrophosphate (Davies et al., 2012; Lin et al., 2001). Whereas (d)ITP and XTP are aberrant nucleotides, IMP and XMP are canonical intermediates of guanosine monophosphate (GMP) synthesis and purine nucleotide catabolism (Heinemann et al., 2021).

Deamination of cytosine to uracil is well known to occur in nucleic acids (Lindahl and Nyberg, 1974; Frederico et al., 1990) but purine bases can also be deaminated. *In vitro*,

the deamination of adenine to hypoxanthine in DNA occurs at 2 to 3% of the rate observed for cytosine to uridine conversion (Lindahl, 1993). The deamination of free nucleotides is less well documented. During heat stress, purine deamination was shown to occur not only in the nucleic acids but also in the pool of free nucleotides (Karran and Lindahl, 1980). In general abiotic stresses, like salinity, water stress, extreme temperature, wounding, UV radiation or the exposure to heavy metals (Corpas et al., 2011; Valderrama et al., 2007) may influence the rate of nucleotide deamination. These stresses generate reactive nitrogen or oxygen species (RNS, ROS) (Corpas et al., 2011; Valderrama et al., 2007) which are mainly discussed in the context of protein modification and lipid peroxidation but are also likely damaging other metabolites although this has rarely been shown so far (Demidchik, 2015).

ITP and dITP are substrates of RNA and DNA polymerases, respectively. Random inosine / deoxyinosine in nucleic acids can thus not only be derived from deamination of adenosine / deoxyadenosine in the polymer but may also be incorporated during the polymerization. When DNA, containing deaminated sites, is replicated, mutations may be introduced. Deoxycytidine can be incorporated opposite of deoxyinosine and often thymidine is placed opposite of deoxyxanthosine (Kamiya, 2003). This misincorportion is not directly detrimental for *Escherichia coli* (Budke and Kuzminov, 2006) because it is rapidly repaired. However, upon stimulation of deamination, the constant deployment of the repair machinery leads to strand breaks and chromosomal rearrangements (Budke and Kuzminov, 2010). By contrast, deoxyinosine in human DNA causes mutations and genome instability even when deamination is not stimulated (DeVito et al., 2017; Yoneshima et al., 2016). In RNA, incorporation of inosine has been shown in non-plant organisms to reduce transcriptional velocity significantly, alter RNA structure and stability and lead to mistranslation (Thomas et al., 1998; Ji et al., 2017). Apart from effects on nucleic acids, ITP and XTP can interfere with various cellular processes like G-protein signaling, microtubule assembly and ATP-dependent metabolic reactions (Muraoka et al., 1999; Klinker and Seifert, 1997; Carnelli et al., 1992). ITP is also a potent inhibitor of the L-glutamic acid decarboxylase in rabbit brain, leading to a decreased synthesis of *γ*-aminobutyric acid (Vanderheiden, 1979) and inhibits the contraction of actomyosine (Burton et al., 2005) in rabbit cells. Furthermore, ITP inhibits

the Topoisomerase II in *Drosophila melanogaster* (Osheroff et al., 1983), and interacts with the F1-subunit of the ATP synthase from *E. coli* (Weber and Senior, 2001).

ITP has been detected *in vivo* in only a few occasions. Human erythrocytes accumulated radioactive ITP after incubation with [^{14}C] adenine, [^{14}C] guanine or [^{14}C] hypoxanthine, indicating that an enzymatic route to deaminated purine nucleotide triphosphates might exist (Fraser et al., 1975). Interestingly, a loss of ITPA function in erythrocytes of mice leads to a substantial accumulation of ITP of up to 10-25% of the ATP pool (Behmanesh et al., 2009). However, erythrocytes are a special cell type which lack nuclear DNA and seem to have a particular nucleotide metabolism. Usually it is technically challenging to detect ITP and XTP at all. In human cancer cells, both were detected with a highly sensitive method in the fmol/mg protein range. Here ITP was around 5 to 10 times more abundant than XTP (Jiang et al., 2018). To date, the corresponding deoxyribonucleotide triphosphates, dITP and deoxyxanthosine triphosphate (dXTP), have never been detected in any organism.

Although these metabolites are low abundant, they can be incorporated into nucleic acids. The frequency of inosine in RNA is about one in 10^5 nucleosides in wild type *E. coli*, while deoxyinosine in DNA is 10-fold less abundant (Pang et al., 2012). This changed in bacteria that harbored a knockout of rdgB, the bacterial ITPA homolog. The inosine content of RNA increased approximately 10-fold and the deoxyinosine of DNA rose about 5-fold compared to the wild type (Pang et al., 2012). These frequencies were elevated even more, to about one inosine per 350 nucleosides in RNA and one deoxyinosine per 1300 nucleosides in DNA, when enzymes involved in purine biosynthesis were lacking whereas the amounts of xanthosine or deoxyxanthosine in nucleic acids barely changed (Pang et al., 2012). In *ITPA* knockout-mice, the inosine to adenosine ratio was about one per 100 nucleosides in RNA (Behmanesh et al., 2009).

In eukaryotes, ITPA deficiency causes drastic phenotypes. In humans it leads to a lethal Martsolf-like syndrome with neurological and developmental abnormalities (Handley et al., 2019). Mice without a functional ITPA had RNA with an elevated inosine content and died shortly after birth with less and abnormally structured sarcomeres (Behmanesh et al., 2009). Bacteria lacking ITPA are viable (Burgis et al., 2003). Recently, a homolog of

ITPA was discovered in *Cassava brown streak virus*, a plant-infecting RNA virus, and was shown to be an important factor during viral infection (Tomlinson et al., 2019).

In this study we identified ITPA of plants and biochemically characterized the enzyme from *A. thaliana* showing that it catalyzes the dephosphorylation of deaminated purine nucleotides. We analyzed mutants of *ITPA* demonstrating that the enzyme safeguards nucleic acids from incorporation of (d)ITP. We were able to detect ITP/IDP accumulation in the mutants and investigated whether the metabolic source for ITP is ATP deamination or spurious IMP phosphorylation. In contrast to *ITPA* mutants in mammals, the Arabidopsis mutants have only minor phenotypic alterations. They show slightly earlier senescence and have elevated concentrations of the defense phytohormone salicylic acid (SA), triggering a transcriptional response of genes associated with SA, systemic acquired resistance and aging.

RESULTS

Identification of an inosine triphosphate pyrophosphatase in plants

An inosine triphosphate pyrophosphatase (ITPA) hydrolyzing deoxyinosine triphosphate (dITP) and inosine triphosphate (ITP) to the respective nucleotide monophosphates and pyrophosphate has not been described for plants so far. Such an enzyme has long been known in bacteria, fungi and mammals (Vanderheiden, 1969; Noskov et al., 1996; Savchenko et al., 2007). We used the amino acid sequence of human ITPA to search with BLASTP for homologs in plants (Supplemental Figure 1). For *Arabidopsis thaliana,* the protein encoded at the gene locus At4g13720 was the only strong homolog. A phylogenetic analysis revealed that ITPA is present in all kingdoms of life including plants and algae (Figure 1, Supplemental Figure 2). Several amino acid residues are highly conserved in ITPAs from different species. Many of these have been shown to be relevant for substrate binding, catalytic activity and dimerization (Supplemental Figure 1, (Stenmark et al., 2007; Gall et al., 2013). For example Phe 153, Ser 180 and Arg 182, which lead to an increased activity with canonical nucleotides like GTP and ATP when mutated in the human enzyme, are highly conserved in all plant ITPAs (Supplemental Figure 2, (Gall et al., 2013). Because of the close similarity of the ITPA enzymes, it is likely that the Arabidopsis enzyme has similar biochemical properties to the human

enzyme, for example regarding substrate specificity and dimer formation. Nonetheless, there are amino acid residues that are only conserved in plant ITPAs (Supplemental Figure 1 and 2). Among these, K/R183 and K/R 189 can be acetylated in Arabidopsis (Liu et al., 2018) but the function of these post translational modifications is unclear.

ITPA has atypical characteristics for an ITP pyrophosphatase

ITPAs are described in other organisms to hydrolyze the phosphoanhydride bond between the alpha and beta phosphate groups of inosine triphosphate resulting in inosine monophosphate (IMP) and pyrophosphate (Figure 2A). To assess the activity of the plant enzyme, a C-terminal Strep-tagged variant of ITPA was transiently expressed in *Nicotiana benthamiana* and affinity purified (Figure 2B). Interestingly, two forms of the protein were purified represented by two bands in a Coomassie-stained SDS-PAGE, possibly indicating a posttranslational modification. The identity of the purified protein was confirmed by immunoblot with an antibody against the Strep-tag. The specific activity of the purified enzyme was measured with several substrates at concentrations of 200 µM, including (deoxy)ribonucleotide di-, and triphosphates, *para*-nitrophenyl-phosphate and nicotinamide adenine dinucleotide (Figure 2C, Supplemental Table 2). An enzymatic activity could only be observed with dITP, ITP, inosine diphosphate (IDP) and xanthosine triphosphate (XTP), as well as with deoxyadenosine diphosphate (dADP) and deoxyguanosine diphosphate (dGDP). In contrast to the ITPA from *H. sapiens* the ITPA of *A. thaliana* efficiently dephosphorylates IDP (Davies et al., 2012). For dITP and ITP the kinetic constants were determined (Figure 2D and E). With ITP as substrate a K_M of 7.1 ± 1.2 µM and a turnover number of 1.9 ± 0.25 s^{-1} were measured. With dITP the K_M was about four-fold lower at 1.7 ± 0.3 µM while the turnover number was similar at 1.5 ± 0.17 s^{-1}. Thus, Arabidopsis ITPA has catalytic efficiencies of 2.6 x 10^5 mM^{-1} s^{-1} for ITP and 8.8 x 10^5 mM^{-1} s^{-1} for dITP (Table 1).

ITPA mutants show an altered phenotype during senescence

To further investigate the role of ITPA *in vivo*, two mutant lines were created. One T-DNA line with an insertion in an exon of *ITPA* was available from the SALK collection (SALK_053023; Figure 3A). We identified plants with a homozygous insertion of the T-DNA and observed that they lacked an intact transcript (Figure 3B). This mutant was

named *itpa-1*. A second line (*itpa-2*) was generated using CRISPR, resulting in a plant with two homozygous single base pair insertions causing frameshifts, one in exon 2 and one in exon 5. From the segregating population harboring the editing construct, *itpa-2* plants without the transgene were selected and used for further characterization. Both mutant lines had no obvious developmental phenotypes (Supplemental Figure 3 A-D) but showed an early onset of senescence at 40 days after germination (Figure 4A) and a slightly increased senescence at an age of eight weeks with around 50% less chlorophyll in the oldest leaves, as well as an increased percentage of dead cells per leaf in *itpa* plants when compared to the wild type (Figure 4B, C and D). The plant fresh weight, the number of seeds per silique and the length of the siliques were not different between the mutants and the wild type (Supplemental Figure 3 B-D).

ITPA is localized in the cytosol, nucleus and plastids

To determine the subcellular localization of ITPA, a transgenic line was generated expressing a C-terminal YFP-tagged variant of ITPA in the *itpa-2* background. In this line ITPA was located in the cytosol, nucleus and chloroplasts in plant leaves (Figure 5A) and in the cytosol and nucleus in roots (Figure 5B). This is in line with the predictions of several bioinformatic analysis tools summarized in the SUBA4 database, predicting nuclear, cytosolic and plastidic localization for ITPA (Hooper et al., 2017). Additionally, ITPA was found in an analysis of the plastid proteome (Kong et al., 2011). A localization in mitochondria also predicted by SUBA4 could not be confirmed in our experiments.

ITPA is essential for the catabolism of ITP and IDP *in vivo*

In 35-day-old plants, IDP and ITP were only detectable in *itpa-1* and *itpa-2* background but not in the wild type (Figure 6A). ITP and IDP were reliably measured because they were baseline separated from the isobaric ATP and ADP isotopes (Supplemental Figure 4). The *itpa-1* and *itpa-2* lines contained 1.7 and 1.8 pmol g^{-1} IDP and 1.8 and 1.3 pmol g^{-1} ITP, respectively. This accounts for about 30 molecules of ITP per 10^6 molecules of adenosine triphosphate (ATP) and between 300 and 400 molecules of IDP per 10^6 molecules of adenosine diphosphate (ADP, Table 2). Per cell the ITP concentration was about 9.6 nM and that of IDP about 11.2 nM estimated according to Straube et al., 2020. Interestingly, the IMP concentration in both knockout lines appears to be lower in

tendency although the data is statistically not significant (Figure 6A). However, the difference in mean IMP concentrations between the wild type and *itpa* plants is by far greater than the sum of ITP and IDP accumulating in the mutants suggesting that ITP/IDP dephosphorylation is not a main contributor to the IMP pool. This is not surprising because IMP is a comparatively abundant intermediate of purine nucleotide biosynthesis and purine nucleotide catabolism (Witte and Herde, 2020; Baccolini and Witte, 2019). Although ITPA is active with dADP and dGDP *in vitro*, mutation of *ITPA* had no effect on the dADP and dGDP concentrations *in vivo* (Supplemental Figure 5A). The concentrations of other purine and pyrimidine nucleotides were also not altered in the mutant lines (Figure 6B, Supplemental Figure 5A-C).

As it has been recently reported that plant viruses infecting *Euphorbiaceae* and especially *Manihot esculenta* (commonly known as Cassava) possess a homologue of ITPA (James et al., 2021; Leiva et al., 2022), we were curious whether ITP and IDP concentrations change during infection with such a virus. We chose to investigate this question in *N. benthamiana* because Arabidopsis is not a known host of viruses encoding ITPA. Three-week-old *N. benthamiana* plants were inoculated with *Cassava Brown Streak Virus* (CBSV) and three weeks after the infection measurements of nucleotides were performed in systemically infected leaves. The concentrations of ITP and IDP increased significantly in the systemically infected leaves (Figure 7A), whereas the concentrations of canonical ribonucleotides did not change (Figure 7B). One has to bear in mind that the ITP and IDP concentrations increased although both ITPases, the viral and the plant ITPA, were present. It appears that viral infection leads to increased ITP / IDP formation that cannot be completely suppressed by the ITPAs.

What is the metabolic source of ITP and IDP?

Hitherto, the metabolic source of ITP / IDP is unknown. One possibility is that these metabolites arise from promiscuous enzyme activity (Hanson et al., 2016) of AMP kinases which in addition to AMP may also be able to phosphorylate IMP. Consistent with this hypothesis, it has been shown in *E. coli* and *Saccharomyces cerevisiae* that an increase of IMP content is concomitant with an accumulation of (deoxy)inosine in RNA and DNA (Pang et al., 2012). Maybe also in plants, more IMP leads to more ITP / IDP, which would indicate that phosphorylation of IMP by kinases is the source of ITP / IDP.

To test this idea, we infiltrated leaves of *N. benthamiana* with ribavirin, an inhibitor of IMP DEHYDROGENASE (IMPDH) (Keya et al., 2003). This enzyme represents a major sink of IMP in plant metabolism (Witte and Herde, 2020) and its inhibition may allow to manipulate the IMP concentration. *N. benthamiana* was chosen, because even in untreated wild type leaves ITP is measurable and thus concentration changes upon treatment can be monitored, whereas in Arabidopsis this metabolite is often only detectable in the *itpa* background (Figure 6A). Ribavirin treatment for two hours caused a significant increase of IMP content in leaves of *N. benthamiana* compared to the mock treatment with buffer (Figure 8). Interestingly, the infiltration itself reduced the IMP concentration. However, the ITP content did not change in any case, and this despite the fact that it was always several orders of magnitude lower than the IMP content. The data show that ITP levels are not directly dependent on IMP concentrations. That the inhibition of IMPDH by ribavirin was successful, was additionally confirmed by the depletion of XMP and GMP in leaves treated with ribavirin – XMP is the product of IMPDH in the pathway of GMP biosynthesis (Supplemental Figure 6).

A biochemical approach was also used to investigate the question of possible aberrant IMP phosphorylation. We determined the enzymatic activities of the two cytosolic AMP kinases, AMPK3 (At5g50370) and AMPK4 (At5G63400) of *A. thaliana* with either 1 mM AMP or IMP as substrates (Lange et al., 2008; Figure 9A and B). Although IMP is an *in vitro* substrate for both enzymes, the activity with IMP was only 3.9% of that with AMP for AMPK3 (Figure 9A) and 5.2% for IMP versus AMP for AMPK4 (Figure 9B). *In vivo* the relative activity with IMP will be by far lower because the cellular IMP pool is several orders of magnitude smaller than that of AMP. Nonetheless, the data show that AMPKs can phosphorylate IMP in principle but overall they indicate that IMP phosphorylation does not contribute strongly to the formation of ITP / IDP.

Aberrant metabolites can also be derived from non-enzymatic processes - from contact with reactive chemicals like ROS (Hanson et al., 2016; Lerma-Ortiz et al., 2016). We wanted to investigate whether ITP can be generated in such a way. Heavy metals are a known source for oxidative damage in plants, for example cadmium, which is often an anthropogenic pollutant (Di Sanità Toppi and Gabbrielli, 1999; Cho and Seo, 2005; Lin et al., 2007). It has been well established that cadmium-induced oxidative stress not only

damages macro molecules such as the DNA directly, but also causes an increased rate of lipid peroxidation (Lin et al., 2007). To test whether this oxidative stress also has an impact on nucleotides, we grew wild type and *itpa-1* plants hydroponically for 14 days and applied cadmium sulfate (0 µM and 10 µM). Without Cd, wild type plants only accumulated small amounts of ITP, but with 10 µM Cd the ITP content rose significantly (Figure 10). IDP was not detectable in the wild type. As expected, the mutant generally contained more IDP and ITP than the wild type and the application of Cd resulted in a further increase of these pools. The concentrations of ITP and IDP measured in this experiment in 14-day-old plants grown in a hydroponic system were comparable to those in 35-day-old plants grown on soil (Figure 6A, Figure 10). Regarding IMP, *itpa-1* plants contained in tendency less of this monophosphate than the wild type irrespective of treatment, similar but more pronounced to what we observed in older plants (Figure 6A). These data show ITP and IDP can be formed under stress conditions that involve ROS probably by deamination of ATP and ADP. Even in the wild type more ITP accumulates due to the stress, indicating either that flux through ITPA is enhanced or that some ITP may not be easily accessible to ITPA, for example ITP generated in the mitochondria. Overall our data suggest that the main source of ITP is not IMP phosphorylation but rather ATP deamination.

ITPA prevents (d)ITP incorporation into DNA and RNA

Measuring deoxyinosine (dI) in digested DNA of 7-day-old plants by liquid chromatography-mass spectrometry (LC-MS) revealed that both mutant lines accumulate deoxyinosine in the DNA (Figure 11A). Wild type DNA contained 290 ± 96 dI per million molecules deoxyadenosine (dA). This amount was more than doubled in the mutants (Supplemental Table 3). In DNA from older plants (56 days) dI could not be detected in the wild type and accumulated in DNA of the mutants to approximately the same level as in seedlings. Therefore, a marked increase of dI accumulation in DNA with age could not be observed. Interestingly, the higher dI concentration in DNA of *itpa* plants demonstrates that a dITP pool must exist but is so small that we are unable to detect it. Deoxyxanthosine was not detected in DNA.

In digested total RNA of 35-day-old plants, 405 ± 117 molecules of inosine per million molecules of adenosine were detected (Figure 11B). The *itpa* lines contained about

twofold more inosine in the RNA (Supplemental Table 3) showing that also the RNA is protected by ITPA. In a preliminary experiment, the RNA of younger, 21-day-old plants was analyzed and contained only 200 molecules inosine per million molecules of adenosine (Supplemental Figure 7), which is about half the amount found in 35-day-old plants. A similar tendency was observed for the *itpa-1* line. In contrast to deoxyinosine in DNA, it appears that the inosine content of RNA increases with age. Interestingly, inosine containing RNA can be specifically recognized and cleaved by an endonuclease in Arabidopsis, which may limit the amount of inosine that can accumulate in RNA (Endo et al., 2021). Xanthosine was not detected in RNA. In summary the data demonstrate that ITPA is an enzyme required to remove dITP and ITP to protect DNA and RNA from random incorporation of (deoxy)inosine (Figure 12).

Loss of ITPA leads to an upregulation of transcripts involved in biotic stress

We further investigated whether the accumulation of (deoxy)inosine in nucleic acids and inosylates in nucleotide pools has an influence on the transcriptome. For this, an RNAseq analysis was performed with RNA isolated from rosette leaves of 35-day-old wild type and *itpa-1* plants that had been grown side-by-side in a randomized fashion and for which we had already confirmed differential levels of inosine in RNA (Figure 11B). Plants lacking ITPA showed an upregulation of 256 transcripts and a downregulation of only 28 transcripts at a $\log_2$ fold change ($\log_2$ FC) of ≥ 2 and ≤ -2 respectively in addition to a false discovery rate (FDR) of ≤ 0.05. Many regulated transcripts were involved in biological processes associated with stress responses and often encode proteins with kinase activity or transcription factors as reported by GO (gene ontology) enrichment analysis (Supplemental Figure 8).

On closer inspection, we found that especially transcripts related to the salicylic acid response (Figure 13A), systemic acquired resistance (SAR, Figure 13B) and aging (Figure 13C) were upregulated. Most prominently transcripts of pathogenesis related 1 (At2g14610), pathogenesis related 2 (At3g57260), pathogenesis related 5 (At1g75040), NIM1 interacting 1 (At1g02450), senescence associated gene 13 (At2g29350), AGD2-like defense response protein 1 (At2g13810), DMR6-like oxygenase 1 (At4g10500) and UDP-dependent glycosyltransferase 76B1 (At3g11340) were differentially regulated. Since the transcriptional profiles suggested that the concentration of stress related

phytohormones may be altered, we quantified salicylic acid (SA), jasmonic acid (JA), jasmonic acid isoleucine (JA-Ile) and abcisic acid (ABA). The concentrations of JA and JA-Ile were not altered and ABA was not detected. However, significantly higher SA concentrations were found in 35-day-old plants lacking ITPA compared to the corresponding wild type (Figure 13D).

DISCUSSION

So far, there have been several sporadic reports about the existence of ITPA in plants (Lin et al., 2001; James et al., 2021), but this enzyme and corresponding mutant plants have not yet been characterized. We show here that plants have ITPA and that the kinetic properties of the enzyme from Arabidopsis are similar to those of the yeast ortholog HAM1p. Interestingly, the human ITPA has a 250-fold higher K_M and a 300 to 500-fold greater catalytic activity than the plant and yeast enzymes (Table 1) which might be an adaptation to high ITP concentrations in some human cells. At least in erythrocytes the ITP pool can be as much as 25% of the ATP pool (Behmanesh et al., 2009), but in other human cells ITP was not detectable (Sakumi et al., 2010).

The K_M of Arabidopsis ITPA for ITP of 7.1 µM is approximately 1000-fold higher than the cellular concentration of ITP (9.6 nM) determined in *itpa* background, which will be even lower in the wild type. We were unable to detect dITP but could show that mutation of *ITPA* led to more deoxyinosine in DNA. Thus, dITP must be an *in vivo* substrate of ITPA (K_M = 1.7 µM for dITP). We estimate that the dITP concentration is in the low pM range assuming that the ratio of ITP to dITP is comparable to the ATP / dATP ratio of about 500 to 1000 ((Straube et al., 2020). A difference of several orders of magnitude between K_M and cellular substrate concentration is also known for other house-keeping enzymes (Michael Y. Galperin et al., 2006; Sakumi et al., 2010). XTP, dXTP and (deoxy)xanthosine in nucleic acids could not be detected indicating that the deamination of (deoxy)guanosine in DNA and RNA and the phosphorylation of (d)XMP are very rare. Therefore, ITPA seems mainly involved with ITP and IDP and somewhat with dITP dephosphorylation *in vivo* (Figure 12). The activity of Arabidopsis ITPA with IDP is interesting, since the yeast and human orthologs have a rather poor activity with IDP (Davies et al., 2012; Holmes et al., 1979). Human cells possess a nudix hydrolase (NUDT16) which hydrolyzes preferably IDP and dIDP, acting synergistically with ITPA to

protect cells from high levels of (d)ITP (Abolhassani et al., 2010). This enzyme is missing in Arabidopsis, which may explain why the plant enzyme is also an efficient diphosphate hydrolase.

According to our data, an important source of ITP is probably the deamination of ATP. This is plausible because the concentration of the adenylates is by far the highest of all nucleotides (Straube et al., 2020) and even a small rate of deamination will generate significant amounts of ITP. Additionally, this rate can be enhanced by oxidative stress, which can occur in plant cells. AMP kinases may also contribute to the IDP / ITP pool because they can use IMP as substrate albeit with lower activity than for AMP. The possibility of spurious phosphorylation by kinases involved in nucleotide metabolism has been discussed recently (Chen et al., 2018; Chen and Witte, 2020). However, *in vivo* there is far more AMP than IMP and our manipulation of IMP in *N. benthamiana* leaves showed no correlation of IMP and ITP concentrations (Figure 8) indicating that the contribution of spurious IMP phosphorylation to the IDP / ITP pools is rather small.

It is surprising that ITPA is only located in the cytosol, nucleus and plastids but not in the mitochondria because ATP occurs in each of these compartments and mitochondria also perform nucleic acid biosynthesis. Additionally, the respiratory chain and photosystems are main sources for ROS in plant cells (Janků et al., 2019), potentially leading to nucleotide and nucleic acid damage, such as nucleotide deamination (Cadet and Wagner, 2013), in mitochondria and plastids, respectively (Tripathi et al., 2020). It is known that ATP and ADP are rapidly exchanged over the mitochondrial membrane because the mitochondria supply the cell with ATP produced by oxidative phosphorylation (Braun, 2020). Therefore, cytosolic ITPA may be able to also purify the mitochondrial adenylate pool – this however implies that ITP and IDP are also rapidly exchanged over the mitochondrial membrane (Haferkamp et al., 2011). By contrast, plastids exchange adenylates with the cytosol mainly at night for ATP import whereas during the day they internally generate ATP from ADP driven by photosynthesis for triosephosphate production. Plastids may require their own ITPA because in the light ROS production is high and adenylates are not exchanged with the cytosol.

Mutant plants of *itpa* show a slightly earlier senescence and increased cell death (Figure 4A - D). This is a relatively moderate phenotype compared to what occurs in mammals.

Mice without functional ITPA die shortly after birth (Behmanesh et al., 2009). A null mutation of *ITPA* in humans leads to severe developmental abnormalities and is also lethal (Handley et al., 2019). Humans with missense mutations in *ITPA* develop severe side effects when treated with purine analoga like ribavirin or thiopurines (Simone et al., 2013). By contrast, the single cell eukaryote *S. cerevisiae* and also the model bacterium *E. coli* show no particular physiological phenotype when they lack ITPA (Clyman and Cunningham, 1987; Pavlov, 1986; Noskov et al., 1996b). Nonetheless, the *E. coli* mutant has an induced SOS response, a pathway that is turned on by DNA damage (Clyman and Cunningham, 1987).

So why do plants lacking ITPA activity show symptoms of early senescence? This may have to do with the accumulation of (deoxy)inosine in DNA and RNA in the mutant (Figure 11, Supplemental Figure 6). Deaminated purines in RNA were shown to lead to reduced polymerase fidelity, RNA structure changes, altered stability and mistranslation (Thomas et al., 1998; Ji et al., 2017), and in case of DNA to mutations (Spee et al., 1993; DeVito et al., 2017) and genome instability (Yoshimura et al., 2007). We observed a higher amount of inosine in RNA of older *itpa* plants (Figure 11, Supplemental Figure 6) indicating that the problems may become more severe with age. DNA damage can lead to programmed cell death (PCD) in Arabidopsis (Wang and Liu, 2006), and we saw a higher incidence of PCD in the *itpa* background during senescence (Figure 4D). An early senescence phenotype similar to that in *itpa* plants was also observed in plants with a higher frequency of unrepaired DNA double-strand breaks (Li et al., 2020). In summary, damage to DNA and RNA by aberrant nucleotide incorporation may well be the cause for the earlier senescence and the increased PCD rate. Alternatively, the detrimental effects of *ITPA* mutation may also be unrelated to the alteration of nucleic acids but caused by ITP accumulation. ITP can directly influence cellular processes that either require or are inhibited by ATP or GTP (Vanderheiden, 1979; Burton et al., 2005; Osheroff et al., 1983; Klinker and Seifert, 1997). However, compared to the sizes of the ATP and GTP pools, the ITP pool is very small even in the *itpa* background, which argues against a direct metabolic interference of ITP.

Recently it has been reported that a viral *ITPA* gene encoded by the *Cassava Brown Streak Virus* (CBSV) is a necrosis determinant (Tomlinson et al., 2019). We could show

that *N. benthamiana* leaves systemically infected with CBSV contained more ITP and IDP (Figure 7A), whereas canonical ribonucleotide levels were not changed when compared to the control plants (Figure 7B). This indicates that the deamination rate of adenylates rises upon viral infection causing an increase of the ITP and IDP pools despite the presence of plant and viral ITPAs. However, viral ITPA likely contributes to limit the inosylate concentration. Whether a high inosylate/adenylate ratio is unfavorable for viral performance requires further investigation.

The abundance of transcripts associated with salicylic acid (SA), senescence and systemic acquired resistance increases in *itpa* plants and they accumulate SA (Figure 13 and Supplemental Figure 8). Mutants with constitutive high levels of SA are known to senesce prematurely. The higher SA levels in *itpa* plants may thus present an explanation for the early senescence phenotype observed (Figure 4A-D) and may also affect plant-pathogen interactions. How the mutation of ITPA and the induction of SA are connected is unclear. We hypothesize that an accumulation of deoxyinosine in DNA causes more DNA repair and turnover associated with occasional double strand breaks. It is known that in plants with more unrepaired DNA double-strand breaks the repair and/or turnover products are sensed and boost SA concentrations (Li et al., 2020). It also has been shown that SA can trigger DNA damage (Hadwiger and Tanaka, 2017) and that proteins involved in DNA damage response, like RAD51, interact synergistically to trigger increased transcription of genes involved in plant immunity (Yan et al., 2013). Taken together it is possible that the transcripts involved in SA response, SAR and aging are upregulated as a consequence of DNA damage.

Another exciting possibility is that ITP or IDP are sensed directly and trigger a response. Such a signaling function has been shown for other nucleotides like extracellular ATP (Cao et al., 2014; Witte and Herde, 2020), NAD/NADH (Pétriacq et al., 2016; Fernie et al., 2020) or the recently discovered 2’,3’-cAMP (Yu et al., 2021) and is speculated for many other nucleotides like mononucleoside polyphosphates, dinucleoside polyphosphates or adenosine-phosphoramidate (Pietrowska-Borek et al., 2020).

Deamination of adenylates is an unavoidable chemical reaction and most organisms including plants have ITPA to protect their nucleic acids from the reaction products.

Whether (d)ITP and (d)IDP are more than just an undesirable metabolic byproduct remains to be investigated.

Material and methods

Plant cultivation

Arabidopsis thaliana (L.) Heynh. plants were grown on soil (Steckmedium, Klasmann) under long-day conditions (Binder KBFW 720 with Osram Lumilux lights,16 h light/8 h darkness, 22°C day, 20°C night, 100 µmol s^{-1} m^{-2} light, 70% humidity). Sown seeds were put on soil in darkness at 4°C for 24 h before being transferred into the growth chamber. *Nicotiana benthamiana* plants were cultivated as described before (Witte et al., 2005).

A segregating T-DNA insertion line from the SALK collection (*itpa*-1, SALK_052023) (Alonso et al., 2003) was acquired from the Nottingham Arabidopsis Stock Centre. A homozygous knockout line and a corresponding wild type were selected from the segregating population.

A second knockout line was obtained via genome editing (*itpa*-2, see Genome editing).

For root-length and germination assays plants were grown in petri dishes containing our in-house medium (Straube et al., 2020; Niehaus et al., 2020).

Plants for the Cadmium sulfate feeding experiment were grown hydroponically according to (Batista-Silva et al., 2019), with small modifications. Plants were grown in in-house liquid medium (Straube et al., 2020; Niehaus et al., 2020) containing 0.4 % agar under long-day conditions (growth chamber with Osram Lumilux lights,16 h light/8 h darkness, 22°C day, 20°C night, 100 µmol s^{-1} m^{-2} light). Jars were filled with 130 ml medium, ensuring that the mesh was not submerged. 10 mg seeds were surface sterilized with 70% ethanol/water for 15 min and subsequently washed with autoclaved water, inverting the reaction tube 2 min and spinning down the seeds for 5 times. Sterilized seeds were taken up in 2 ml 0.15% (w/v) agarose in water and diluted to a final concentration of 2.5 mg ml^{-1} seeds with the agarose solution. The solution was mixed and one milliliter per mesh was spread evenly. Cadmium treatment was performed for 24h by adding a 500 mM cadmium sulfate solution to a final concentration of 10 µm to the medium, respectively. This concentrations was chosen according to (Di Sanità Toppi and

Gabbrielli, 1999), as we aimed for physiologically and environmentally relevant concentrations.

DNA extraction, RNA extraction, genotyping and cloning

DNA for genotyping was isolated according to the BOMB-protocol using the TNA extraction from plants with TNES/GITC lysis protocol (Oberacker et al., 2019). Magnetic beads were silica-coated beads, synthesized using the BOMB protocol for coating ferrite magnetic nano particles with silica oxide (Oberacker et al., 2019).

Total RNA was isolated using the Plant NucleoSpin II kit (Macherey-Nagel) according to manufacturer's specifications.

Primers used in this study can be found in Supplemental Table 4.

Arabidopsis T-DNA insertion mutants (*itpa-1*) and respective wild type plants were identified by PCR using the following primer combinations: P1628 and P1629 (wild type reaction); P1628 and P1316 (T-DNA reaction). The PCR product of the T-DNA reaction was send for sequencing. The T-DNA insertion was found to be positioned as described on the Signal website (http://signal.salk.edu/cgi-bin/tdnaexpress). Gene-specific mRNA level were determined by extracting total RNAs from seedlings of wild type and knockout plants and subsequent reverse transcription (Revert Aid H Minus first strand cDNA synthesis kit, ThermoFisher). PCRs were facilitated using T-DNA insertion flanking primers P2487 and P2488. An amplification of *actin2* was used as control with the primers 1033 and 1034. The PCR was carried out with 35 cycles using an annealing temperature of 55°C.

The ITPA coding region was amplified from cDNA using the primers P1075 and P1076. The restriction sites EcoRI and XmaI were introduced via the primers and the fragment was cloned into pXCScpmv-HA-Strep (V69) (Claus-Peter Witte et al., 2004) for protein production and into pXCS-YFP (V36) (Myrach et al., 2017; Dahncke and Witte, 2013) for localization studies.

Generation of *itpa-2* by genome editing

Vectors for CRISPR-induced editing of the ITPA encoding locus At4g13720 were constructed as previously described (Rinne et al., 2021). We used two gRNAs (target

sequences: TGAGCTCCAAGGTGAGCCTG; CTAGAGAAGCTTGGTCACGA), each expressed by an AtU6-26-promoter on the same vector. The final vector contained (I) Selectable phosphinotricin resistance cassette encoding a phosphinotricin acetyltransferase; (II) Cas9 under the controle of the EC1.2-promoter for egg cell-specific Cas9-expression (Wang et al., 2015); (III) the gRNA-expression cassette and (IV) green fluorescent protein (GFP) expressed by seed specific At2S3-promoter (Aliaga-Franco et al., 2019) for selection of non-glowing T-DNA-free seeds. The vector was transformed into *Agrobacterium tumefaciens* strain AGL-1. *Arabidopsis thaliana* Col-0 plants were grown as described above until flowers developed and transformed by floral dip (Clough and Bent, 1998). T1 seeds were harvested and screened for transgenicity by spraying 1:1000 diluted phosphinotricin (BASTA®, Bayer). Resistant plants were grown until seeds developed and T2-seedlings were genotyped for mutations in the ITPA locus. Genotyping was performed via amplified fragment length polymorphism (AFLP) analysis of the genomic area around the targeted sites as described previously (Rinne et al., 2021). The first target site located in the second exon was amplified with P1774 and P1775 and the second target site located in the fifth exon was amplified with P1776 and P1777. Mutations were confirmed by Sanger sequencing (Microsynth-Seqlab). Plants harboring mutations in the ITPA locus were grown further until seeds developed. To obtain T-DNA-free T3 seeds, non-glowing seeds were selected and germinated. Absence of the T-DNA was confirmed by PCR-amplification with P1164 and P1165 and inheritance of mutations in the ITPA locus were confirmed by Sanger sequencing. Plants that showed no DNA-amplification with T-DNA-specific oligonucleotides were used for further experiments.

Protein purification, quantification and enzymatic assay

C-terminal strep-tagged ITPA, AMPK3 and 4 (Chen et al., 2018) were transiently overexpressed in *N. benthamiana* and affinity purified after five days as described before (Werner et al., 2008). Briefly, a clarified extract from 0.75 g leaves was incubated with 40 µl Streptactin-Macroprep (50% slurry, IBA GmbH, Germany). The Macroprep was washed five times with washing-buffer and eluted in 150 µl elution-buffer. The amount of protein was determined by an in-gel quantification assay using known concentrations of bovine serum albumin as a standard and Li-cor Odyssey FC with Image Studio software.

SDS gel electrophoresis and Coomassie Brilliant Blue R250 staining was performed as described previously (Claus-Peter Witte et al., 2004).

Enzymatic assays for ITPA were performed using the EnzChek™ Pyrophosphate Assay Kit (ThermoFisher scientific) according to manufacturer's instructions, with the exception of reducing the volume of all solution to one fifth of the instructions using High Precision Cells (Hellma Analytics). The enzymatic activity was measured at 360 nm using an UV-2700 UV-Vis-spectrophotometer (Shimadzu). Resulting data were analyzed with Graph Pad Prism 4, determining kinetic constants fitting the data to the Michaelis-Menten equation. Specific activities were screened with 200 µM of the respective substrate, enzymatic constants for ITP were determined using concentrations of 1.5, 3.0, 6.25, 12.5, 25.0 and 50.0 µM ITP; for dITP concentrations of 1, 3, 6, 15, and 30 µM dITP were used.

AMPK3 and 4 activity was determined using a coupled enzyme assay with pyruvate kinase and lactate dehydrogenase (LDH, Sigma, P0294), measuring the production of NAD^+ that results in absorption-decrease at 340 nm (AMPK3) or 1 µl purified enzyme (AMPK4) were used in a total volume of 300 µl containing 40 mM Tris-SO_4, 20 mM KCL, 4 mM $MgCl_2$, 2 mM phosphoenolpyruvate, 0.17 mM NADH, 2 µl 1:50 diluted coupling enzyme solution (600-1000 U/ml PK and 900-1400 U/ml LDH). The reaction was started by adding ATP to a final concentration of 1 mM and measured by a microplate spectrophotometer (Multiskan GO, Thermo Scientific) at 22°C for 20 min. The absorption change was calculated from the linear phase and subtracted by the change in a blank-sample, containing everything but the substrate. Absolute amounts were calculated utilizing the Beer-Lambert law.

Subcellular localization

A construct leading to the expression of ITPA, c-terminally fused to YFP, was transformed into *A. thaliana* via floral dipping (Clough and Bent, 1998). T1 seeds were harvested and screened for transgenicity by spraying 1:1000 diluted phosphinotricin (BASTA®, Bayer). Resistant plants were grown until seeds developed and T2-seedlings were grown and screened for fluorescence. Whole leaves or roots were taken and immersed in octadecafluor-decahydronaphthalin (Sigma-Aldrich, (Littlejohn et al., 2010)).

The samples were analyzed using a Leica True Confocal Scanner SP8 microscope equipped with an HC PL APO CS2 40 × 1.10 water immersion objective (Leica, Germany) as described in (Dahncke and Witte, 2013). The acquired images were processed using Leica Application Suite Advanced Fluorescence software (Leica Microsystems).

Metabolite analysis

The analysis of nucleotide concentration was performed as recently described with slight modifications (Straube et al., 2020). Briefly, around 250 mg *Arabidopsis* rosette leaves of five-weeks-old plants were isolated with 15% trichloroacetic acid, the cleared supernatant was neutralized and extracted by a liquid-liquid extraction employing a mixture of 78%/ 22% dichloromethane/ trioctylamine and passed through a weak anion-exchange solid phase extraction cartridge (Strata-X-AW; Phenomenex). Dried extracts were resolved in 25 µl 5 mM ammonium acetate in water, pH 9.5. For HPLC-MS an Agilent 1290 Infinity II LC System coupled with an Agilent 6470 triple quadrupole mass spectrometer was used employing a porous graphitized black chromatography. The source parameters were employed as stated before (Straube et al., 2020), but chromatographic parameters for the hypercarb chromatograph were changed as follows: The chromatography was performed using a flowrate of 0.6 ml min^{-1} and a column temperature of 35°C. The injection volume was increased to 20 µl. An adapted hypercarb gradient was utilized: 0 min, 100% A; 3 min, 100% A; 18 min, 70% A; 19 min, 0% A; 22 min, 0% A; 22.5 min, 100% A until 30 min. Transitions (precursor ions and product ions), fragmentor and collision energies employed for dITP, IDP, ITP, XMP and XTP are shown in Table 3. The concentration of ATP and IMP was determined using the isotope dilution technique (Kuskovsky et al., 2019; Straube et al., 2020), while ADP, IDP, ITP and XMP were quantified by an external calibration curve in the respective plant matrix. Only calibration curves with an R^2-value >0.99 were accepted. Depictions of the standard for IDP and ITP in buffer or matrix, as well as the wild type and knockout results can be found in the supplemental materials (Supplemental Figure 4). Phytohormones were extracted and measured according to (Cao et al., 2014; Yang et al., 2017). Briefly, 100 mg plant material was quickly harvested in 2 ml safe lock tubes containing 12 2-mm steel beads and flash frozen. Samples were ground in a mixer mill

for 1 min at 30 Hz. Subsequently 1 ml ethylacetate was added, containing isotope standard (D4-salicylic acid, D6-absicic acid, D6-jasmonic acid, D6-jasmonic acid isoleucine) and samples with buffer were ground again for 1 min at 30 Hz. Then, samples were centrifuged for 40000 x *g* at 4°C for 10 min. The supernatant was taken and dried in a vacuum centrifuge. The pellet was resuspended in 300 µl 0.1% formic acid in 70/ 30 water/ methanol by inverting the reaction tubes at 4°C for 10 min. LC-MS analysis was performed on an Agilent 1290 Infinity II LC System coupled with an Agilent 6470 triple quadrupole mass spectrometer. Chromatography was performed employing a 100 x 2.1 mm Accucore Phenyl Hexyl column (Thermo Scientific) with a particle size of 2.6 µm. The injection volume was set to 5 µl, column temperature to 30°C and the flowrate was 0.4 ml min^{-1}. Mobile phase A was 0.1% formic acid in water and mobile phase B was 0.1% formic acid in methanol. The gradient was set as follows: 0 min, 60% A; 3 min, 45% A; 5 min, 0% A; 6 min, 0% A, 6.1 min, 60% A until 13 min. In-source parameters were set to: Gas temperature 300°C, gas flow 5 L min−1, nebulizer pressure 30 psi, sheath gas temperature 300°C, sheath gas flow 11 L min−1, capillary voltage 3000 V, and nozzle voltage 1000 V. All analytes were measured in negative mode, transitions (precursor ions and product ions), fragmentor and collision energies employed for analysis are shown in Table 4.

Quantitative determination of (deoxy)inosine/(deoxy)adenosine level in total RNA and DNA

DNA was extracted using a modified CTAB- (heydecyltrimethylammonium bromide) based protocol. Briefly, 1 g plant material was frozen in liquid nitrogen and ground in a mortar with 50 mg polyvinylpolypyrrolidone. 1.5 ml CTAB Buffer (2% CTAB; 20 mM EDTA; 1.4 M NaCl; 150 mM Tris-HCL pH 7.5) were added and the material was thawed with occasional gentle stirring, transferred to 2 x 2 ml reaction tubes and placed in a water bath for 10 min at 60°C. 0.5 ml chloroform:isoamylacohol (24:1) was then added and the tubes were inverted 10 times. The tubes were centrifuged at room temperature for 5 min at 21000 x *g* and the supernatant was transferred to a new 2 ml tube containing 0.5 ml phenol:chloroform:isoamylacohol (25:24:1). This solution was inverted thoroughly and centrifuged as stated before. The phenol-step was repeated and the resulting supernatant was transferred to a tube containing 0.5 ml chloroform, inverted and centrifuged for 3 min at room temperature at 21000 x *g*. The supernatant was then

pooled in a 2 ml reaction tube and 0.6 times the volume of isopropanol was added and centrifuged at 21000 x *g* for 2 min to precipitate the nucleic acids. The supernatant was discarded and the pellet was resolved in 600 µl TE buffer (5 mM, pH 7.5) containing 50 µg/ml RNAse A and incubated at 60 °C for 10 min in a water bath. Precipitates were removed by centrifugation at 21.000 x *g* for 3 min. 60 µl 3 M sodium acetate (pH 5.2) and 1.2 ml ethanol were added to the supernatant and the supernatant was spun down at 21000 x *g* for 5 min to precipitate the DNA. The pellet was washed with 70% ethanol and resuspended in 100 µl Tris buffer (5 mM). Nucleic acids concentrations were determined using a spectrophotometer (Nanophotometer, Implen).

Nucleic acids were digested using the Nucleoside Digestion Mix (NEB) with the following modifications: 5 µl Nucleoside Digestion Mix Reaction Buffer (10X) and 0.5 µl Nucleoside Digestion Mix were used, adding RNA/DNA and water depending on the respective concentration of the RNA/DNA up to a total volume of 50 µl. The mixture was incubated for 4 h at 37°C. A total of 1 µg RNA or 3 µg DNA was digested.

Digested RNA and DNA was measured by HPLC-MS using the stated setup but different chromatographic and source parameters as recently published (Franziska R. Traube et al., 2019). A Poroshell 120 SB-C18 (2.7 µm, 2.1 × 150 mm; Agilent Technologies) was employed for chromatographic separation using a gradient employing solvent A (0.0075% formic acid in water) and solvent B (0.0075% formic acid in methanol) (0-3min min, 0% solvent B; 3.0-8.0 min 11% solvent B; 8.0-8.25 min, 50% solvent B; 8.25-10.25 min, 50% solvent B; 10.25-10.50 min, 0% solvent B until 13.5 min). A flowrate of 0.35 ml/min was applied and 10 µl digested RNA were injected. The source parameter were set as following: Positive mode, gas temperature 80°C, gas flow 13 L/min, nebulizer 30 psi, sheath gas temperature 275°C, sheath gas flow 11 L/min, capillary voltage 2500 V and nozzle voltage 500 V.

Analysis of chlorophyll content

Measurement of chlorophyll content was performed as described previously (Harris and Baulcombe, 2015). Three leaf discs (4 mm radius) were taken from the three oldest leaves of eight-weeks-old plants and extracted in 1 ml dimethylformamide (DMF) over night at 4°C. This was done for 5 plants. 300 µl extract were diluted with 600 µl and the

absorbance (A) at 647 nm and 664.5 nm was measured with a spectrophotometer (Nanophotometer, Implen) in a glass cuvette. Chlorophyll content per mm^2 was calculated as follows:

$$\frac{\left(\left((12 * A_{664.5}) - (2.79 * A_{647})\right) + \left((20.78 * A_{647}) - (4.88 * A_{664.5})\right)\right)}{3 * \pi * 4^2} = chlorophyll\ (\frac{\mu g}{mm^2})$$

Cell death staining

Trypan blue staining was performed as published recently (Nuria Fernández-Bautista et al., 2016). Briefly, the oldest, fully developed leaves of 56-days-old plants were harvested and stained by a staining solution (10 ml lactic acid (85% w/w), 10 ml equilibrated phenol, pH 7.5-8.0, 10 ml glycerol, 10 ml distilled water, total concentration of 10 mg/ml trypan blue) for an hour. The staining solution was removed and leaves were covered with 100% ethanol. This ethanol was changed until the leaves became completely destained. The ethanol was removed and leaves were stored in 60% glycerol.

Cell death quantification

To quantify the leaf area affected by cell death, RGB pictures of stained leaves were taken and opened with ImageJ. A binary picture was created splitting the color channels (Image → color → split channels). The red channel was further processed for measuring the area of dead cells. The contrast was enhanced by 0.1% (process → enhance contrast). Then a minimum filter was applied, followed by a maximum filter, both with a radius of 10 pixel. Afterwards a threshold was set and particles were analyzed (radius of 3 – infinite pixel). All picked spots were measured. For total leaf area, the blue channel was processed by first increasing the contrast by 0.1% and then applying a minimum filter followed by a maximum filter, both with a radius of 50 pixel. A threshold was set and the area was measured. The area of dead cells was divided by the total leaf area and multiplied by 100, resulting in a percentage area of dead cells per total leaf area.

Sequence Analysis and Phylogenetic Analysis

ITPA sequences were identified using the Phytozome v12.1 webserver (https://phytozome.jgi.doe.gov/pz/portal.html) and the National Center for Biotechnology

(NCBI) for all non-plant organisms employing BLASTP searches with the *Arabidopsis* amino acid sequence. Alignments were generated using the Muscle algorithm in MEGAX. The alignment was used to construct a maximum likelihood tree using MEGAX (Kumar et al., 2018). Initial tree(s) were obtained automatically by applying Neighbor-Join and BioNJ algorithms to a matrix of pairwise distances estimated using a JTT model, and then selecting the topology with superior log likelihood value (-5225.0). All positions with less than 95% coverage were eliminated, resulting in 173 positions in the final dataset. A discrete Gamma distribution was used to model evolutionary rate differences among sites (5 categories (+G, parameter = 0.9102)). Numbers at branches indicate the percentage of trees in which associated taxa clustered together and were calculated by a bootstrap analysis (1000 bootstraps). The alignment used to construct the phylogenetic tree can be found in Supplemental Figure 2. Conserved residue shading was performed using Boxshade (http://www.ch.embnet.org/software/BOX_form.html). Conserved domains were identified using information from crystallography studies of the human ITPA (Stenmark et al., 2007), as well as bioinformatics analysis using the Conserved Domain Database (Lu et al., 2020). Abbreviations and loci used for the phylogenetic analysis are as follows (Phytozome V12.1 locus identifiers for plant and algae sequences and NCBI locus identifiers for non-plant sequences are given): *Asp nig*, *Aspegillus niger* (XP_001398459.1); *Ara tha*, *Arabidopsis thaliana* (At4g13720); *Bac sub*, *Baccillus subitilis* (OIS57636.1); *Bot cin*, *Botrytis cinerea* (XP_024547817.1); *Cae ele*, *Caenorhabditis elegans* (NP_498121.1); *Chl rei*, *Chlamydomonas reinhardtii* (Cre02g095089.t1.1); *Dan rer*, *Danio rerio* (NP_001093456.1); *Dei rad*, *Deinococcus radiodurans* (WP_010886825.1); *Dro mel*, *Drosophila melanogaster* (NP_608890.1); *Esc col*, *Escherichia coli* (NAA10980.1); *Gal gal*, *Gallus gallus* (NP_001258859.1); *Gly max*, *Glycine max* (Glyma10G125100.1); *Hom sap*, *Homo sapiens* (AAK21848.1); *Mar pol*, *Marchantia polymopha* (Mapoly0026s0018.1); *Met jan*, *Methanocaldococcus jannaschii* (WP_064496428.1); *Med tru*, *Medicago truncatula* (Medtr1g047390.1); *Neu cra*, *Neurospora crassa* (XP_955963.1); *Ory sat*, *Oryza sativa* (Os10g31940.1); *Phy pat*, *Physcomitrium patens* (Pp3c16_19640V3.1); *Pha vul*, *Phaseolus vulgaris* (Phvul.007G236950.1); *Sac cer*, *Saccharomyces cerevisiae* (AJR66682.1); *Sel moe*, *Selangiella moellendorffii* (e_gw1.0.2702.1); *Sol lyc*, *Solanum lycopersicum*

(Solyc09g091420.2.1); *Sol tub*, *Solanum tuberosum* (PGSC0003DMT400076168); *Sus scr*, *Sus scrofa* (XP_020933236.1); *Tri aes*, *Triticum aestivum* (KAF6994464); *Ust may*, *Ustilago maydis* (XP_011387918.1); *Vol car*, *Volvox carteri* (Vocar0027s0182.1); *Xen lae*, *Xenopus laevis* (XP_018114098.1); *Zea may*, *Zea mays* (GRMZM2G020295_T02).

RNAseq analysis

Total RNA from 35-days-old rosette leaves from *A. thaliana* Col-0 (‘wild type‘) and *itpa*-1 plants were send for Illumina mRNA sequencing to Novogene (Cambridge, United Kingdom). cDNA libraries were sequenced with 2x150 bp read length in *paired-end* mode. The total coverage of each sample is given in Table 5. Initial quality control of raw reads was performed with FastQC v0.11.9 (Andrews, 2010). After passing the quality control, reads were mapped to the *A*. *thaliana* (TAIR10) genome with CLC Genomics Workbench v20.0.03 using default parameters. For this, the RNAseq-mapping algorithm was used. Genes with following criteria were selected as differential expressed genes (DEG): $\log_2$ fold change ($\log_2$FC) ≥ 2, ≤ -2 (*itpa-1/*wild type); false discovery rate (FDR) ≤ 0.05 (Benajmin Hochberg correction). Log_2(reads per kilobase of model, RPKM) values were calculated as expression values. Single enrichment analysis (SEA) was done with the webtool agriGO v2.0 (Tian et al., 2017) for up- and down-regulated DEGs with the following parameters: Selected species: *Arabidopsis thaliana*; Reference: TAIR genome locus (TAIR10_2017); Statistical test method: Hypergeometric; Multi-test adjustment method: Hochberg (FDR); Significance level: 0.01; Minimum number of mapping entries: 10; Gene ontology type: Complete GO. A summary of DEGs and the results of the GO term enrichment analysis can be found in Supplemental Table 5 and 6, respectively.

Viral infection

The original freeze-dried CBSV inoculum PV-0925 was obtained from the Leibniz-Institut DSMZ - Deutsche Sammlung von Mikroorganismen und Zellkulturen GmbH (Braunschweig, Germany). The three oldest leaves of three-weeks-old *Nicotiana benthamiana* plants were treated with buffer (0.05 M KH_2PO_4, 0.05 M Na_2HPO_4, 1 mM EDTA, 5 mM sodium diethyldithiocarbamate, a spatula tip of active coal and Celite 545) or with buffer containing 15 5 mm per 5 ml buffer leaflets (non-necrotic but symptomatic)

of Cassava brown streak virus infected plants by mechanical inoculation. The youngest, systemically infected leaves were harvested 21 days after infection.

Ribavirin treatment

The first fully developed true leaves of three-weeks-old *Nicotiana benthamiana* plants were fully inoculated with buffer (10 mM 2-(N-morpholino)ethanesulfonic acid, 10 mM $MgCl_2$, pH 5.6) or buffer containing 500 µM ribavirin (1-[(2R,3R,4R,5R)-3,4-Dihydroxy-5-hydroxymethyl-oxolan-2-yl]-1,2,4-triazol-3-carboxamid) in buffer. Samples were harvested after 2 h.

Statistical analysis

Statistical analysis for the determination of kinetic constants was performed using GraphPad Prism 4. For metabolite data, the R software (version 1.2.5042) and CRAN packages multcomp and sandwich were used to perform two-sided Tukey's pairwise comparisons and to consider heteroscedasticity of the dataset with the sandwich variance estimator (Herberich et al., 2010). Number of replicates, test values and multiplicity-adjusted p values are reported in the Supplemental Table 1.

Figure design

All figures were designed to be colorblind safe and display the numbers behind the visualization as accurate as possible using "COLORBREWER 2.0. Color advice for cartography"; https://colorbrewer2.org/#.

ACCESSION NUMBERS

Information about the mutant lines in this article can be obtained in the GenBank/EMBL data libraries under the following accession number:

At4g13720 (ITPA).

SUPPLEMENTAL DATA

Supplemental Table 1. Raw and statistic data

Supplemental Table 2. Substrates tested for biochemical activity with ITPA

Supplemental Table 3. Ratios (deoxy)inosine per million molecules (deoxy)adenosine in DNA and RNA, respectively

Supplemental Table 4. List of primers used in this study

Supplemental Table 5. List of differentially expressed genes

Supplemental Table 6. List of the GO term enrichment analysis

Supplemental Figure 1. Comparative sequence analysis of inosine triphosphate pyrophosphatases

Supplemental Figure 2. Comparative sequence analysis of inosine triphosphate pyrophosphatases from several phylogenetically distant model organisms of all kingdoms of life

Supplemental Figure 3. Phenotyping of wild type and *itpa* mutant plants

Supplemental Figure 4. Chromatograms of ITP and IDP analyzed by hypercarb chromatography

Supplemental Figure 5. Relative concentration of different nucleotides in rosette leaves of 35-day-old wild type and itpa mutant plants

Supplemental Figure 6. Manipulation of IMP content in leaves of N. benthamiana alters the concentration of GMP and XMP, and in tendency also GTP

Supplemental Figure 7. Concentration of inosine in isolated RNA of wild type and itpa-1 plants

Supplemental Figure 8. Loss-of-function of ITPA leads to differential upregulation of transcripts associated with GO:terms of biological processes, molecular functions and cellular components

ACKNOWLEDGEMENT

We would like to express our gratitude to Holger Eubel and Björn Heinemann for providing the hydroponic system and André Specht for technical assistance. We also like to thank Anke Steppuhn (University of Hohenheim) for the donation of the phytohormone isotope standards. We furthermore like to express our gratitude to Sören Budig and Frank Schaarschmidt (Leibniz University, Hannover) for advice on the statistical analysis.

AUTHOR CONTRIBUTIONS

HS and MH designed the study, HS, JS, JR, MN and HR acquired experimental data, HS, JS, JR and MH analyzed the data and HS, CPW and MH interpreted the data. HS, CPW and MH wrote the manuscript, all authors read and revised the manuscript and agreed on the final version.

FUNDING

This work was supported by the Deutsche Forschungsgemeinschaft (HE 5949/4-1 to M.H.), (grant no. WI3411/7-1 and WI3411/8-1 to C-P.W.), and (grant no. INST 187/741-1 FUGG).

Conflict of interest statement. None declared.

DATA DEPOSITION

Raw read data from Illumina sequencing is deposited at the Sequence Read Archive (SRA) on NCBI under following accession number: PRJNA807491.

REFERENCES

Abolhassani, N., Iyama, T., Tsuchimoto, D., Sakumi, K., Ohno, M., Behmanesh, M., and Nakabeppu, Y. (2010). NUDT16 and ITPA play a dual protective role in maintaining chromosome stability and cell growth by eliminating dIDP/IDP and dITP/ITP from nucleotide pools in mammals. Nucleic Acids Research **38** (9): 2891–2903.

Aliaga-Franco, N., Zhang, C., Presa, S., Srivastava, A.K., Granell, A., Alabadí, D., Sadanandom, A., Blázquez, M.A., and Minguet, E.G. (2019). Identification of transgene-free CRISPR-edited plants of rice, tomato, and arabidopsis by monitoring DsRED fluorescence in dry seeds. Frontiers in Plant Science **10**: 1150.

Alonso, J.M., Stepanova, A.N., Leisse, T.J., Kim, C.J., Chen, H., Shinn, P., Stevenson, D.K., Zimmerman, J., Barajas, P., Cheuk, R., Gadrinab, C., Heller, C., Jeske, A., Koesema, E., Meyers, C.C., Parker, H., Prednis, L., Ansari, Y., Choy, N., Deen, H., Geralt, M., Hazari, N., Hom, E., Karnes, M., Mulholland, C., Ndubaku, R., Schmidt, I., Guzman, P., Aguilar-Henonin, L., Schmid, M., Weigel, D., Carter, D.E., Marchand, T., Risseeuw, E., Brogden, D., Zeko, A., Crosby, W.L., Berry, C.C., and Ecker, J.R. (2003). Genome-wide insertional mutagenesis of Arabidopsis thaliana. Science **301** (5633): 653–657.

Andrews, S. (2010). FastQC: A Quality Control Tool for High Throughput Sequence Data. Available online at: http://www.bioinformatics.babraham.ac.uk/projects/fastqc/

Baccolini, C., and Witte, C.-P. (2019). AMP and GMP catabolism in arabidopsis converge on xanthosine, which is degraded by a nucleoside hydrolase heterocomplex. The Plant Cell **31** (3): 734–751.

Batista-Silva, W., Heinemann, B., Rugen, N., Nunes-Nesi, A., Araújo, W.L., Braun, H.-P., and Hildebrandt, T.M. (2019). The role of amino acid metabolism during abiotic stress release. Plant, Cell & Environment **42** (5): 1630–1644.

Behmanesh, M., Sakumi, K., Abolhassani, N., Toyokuni, S., Oka, S., Ohnishi, Y.N., Tsuchimoto, D., and Nakabeppu, Y. (2009). ITPase-deficient mice show growth retardation and die before weaning. Cell death and differentiation **16** (10): 1315–1322.

Braun, H.-P. (2020). The oxidative phosphorylation system of the mitochondria in plants. Mitochondrion **53**: 66–75.

Budke, B., and Kuzminov, A. (2006). Hypoxanthine incorporation is nonmutagenic in Escherichia coli. Journal of Bacteriology **188** (18): 6553–6560.

Budke, B., and Kuzminov, A. (2010). Production of clastogenic DNA precursors by the nucleotide metabolism in Escherichia coli. Molecular Microbiology **75** (1): 230–245.

Burgis, N.E., Brucker, J.J., and Cunningham, R.P. (2003). Repair system for noncanonical purines in Escherichia coli. Journal of Bacteriology **185** (10): 3101–3110.

Burton, K., White, H., and Sleep, J. (2005). Kinetics of muscle contraction and actomyosin NTP hydrolysis from rabbit using a series of metal-nucleotide substrates. The Journal of Physiology **563** (Pt 3): 689–711.

Cadet, J., and Wagner, J.R. (2013). DNA base damage by reactive oxygen species, oxidizing agents, and UV radiation. Perspectives in Biology **5** (2).

Cao, Y., Tanaka, K., Nguyen, C.T., and Stacey, G. (2014). Extracellular ATP is a central signaling molecule in plant stress responses. Current Opinion in Plant Biology **20**: 82–87.

Carnelli, A., Michelis, M.I. de, and Rasi-Caldogno, F. (1992). Plasma Membrane Ca-ATPase of Radish Seedlings I. Biochemical characterization using ITP as a substrate. Plant Physiology **98** (3): 1196–1201.

Carole L Linster, Emile Van Schaftingen, and Andrew D Hanson (2013). Metabolite damage and its repair or pre-emption. Nature Chemical Biology **9** (2): 72–80.

Chen, M., Urs, M.J., Sánchez-González, I., Olayioye, M.A., Herde, M., and Witte, C.-P. (2018). m6A RNA degradation products are catabolized by an evolutionarily conserved N6-Methyl-AMP deaminase in plant and mammalian cells. The Plant Cell **30** (7): 1511–1522.

Chen, M., and Witte, C.-P. (2020). A kinase and a glycosylase catabolize pseudouridine in the peroxisome to prevent toxic pseudouridine monophosphate accumulation. The Plant Cell **32** (3): 722–739.

Cho, U.-H., and Seo, N.-H. (2005). Oxidative stress in Arabidopsis thaliana exposed to cadmium is due to hydrogen peroxide accumulation. Plant Science **168** (1): 113–120.

Claus-Peter Witte, Laurent Noël, Janine Gielbert, Jane Parker, and Tina Romeis (2004). Rapid one-step protein purification from plant material using the eight-amino acid StrepII epitope. Plant Molecular Biology **55** (1): 135–147.

Clough, S.J., and Bent, A.F. (1998). Floral dip: a simplified method for Agrobacterium-mediated transformation of Arabidopsis thaliana. The Plant Journal for Cell and Molecular Biology **16** (6): 735–743.

Clyman, J., and Cunningham, R.P. (1987). Escherichia coli K-12 mutants in which viability is dependent on recA function. Journal of Bacteriology **169** (9): 4203–4210.

Corpas, F.J., Leterrier, M., Valderrama, R., Airaki, M., Chaki, M., Palma, J.M., and Barroso, J.B. (2011). Nitric oxide imbalance provokes a nitrosative response in plants under abiotic stress. Plant Science **181** (5): 604–611.

Crécy-Lagard, V. de, **Haas, D., and Hanson, A.D.** (2018). Newly-discovered enzymes that function in metabolite damage-control. Current Opinion in Chemical Biology **47**: 101–108.

Dahncke, K., and Witte, C.-P. (2013). Plant purine nucleoside catabolism employs a guanosine deaminase required for the generation of xanthosine in Arabidopsis. The Plant Cell **25** (10): 4101–4109.

Davies, O., Mendes, P., Smallbone, K., and Malys, N. (2012). Characterisation of multiple substrate-specific (d)ITP/(d)XTPase and modelling of deaminated purine nucleotide metabolism. BMB Reports **45** (4): 259–264.

Demidchik, V. (2015). Mechanisms of oxidative stress in plants: From classical chemistry to cell biology. Environmental and Experimental Botany **109**: 212–228.

DeVito, S., Woodrick, J., Song, L., and Roy, R. (2017). Mutagenic potential of hypoxanthine in live human cells. Mutation Research **803-805**: 9–16.

Di Sanità Toppi, L., and Gabbrielli, R. (1999). Response to cadmium in higher plants. Environmental and Experimental Botany **41** (2): 105–130.

Dobrzanska, M., Szurmak, B., Wyslouch-Cieszynska, A., and Kraszewska, E. (2002). Cloning and characterization of the first member of the Nudix family from Arabidopsis thaliana. Journal of Biological Chemistry **277** (52): 50482–50486.

Dubois, E., Córdoba-Cañero, D., Massot, S., Siaud, N., Gakière, B., Domenichini, S., Guérard, F., Roldan-Arjona, T., and Doutriaux, M.-P. (2011). Homologous recombination is stimulated by a decrease in dUTPase in Arabidopsis. PLoS ONE **6** (4): e18658.

Fernie, A., Hashida, S.-N., Yoshimura, K., Gakière, B., Mou, Z., and Pétriacq, P. (2020). Editorial: NAD Metabolism and Signaling in Plants. Frontiers in Plant Science **11**: 146.

Fraser, J.H., Meyers, H., Henderson, J.F., Brox, L.W., and McCoy, E.E. (1975). Individual variation in inosine triphosphate accumulation in human erythrocytes. Clinical Biochemistry **8** (1-6): 353–364.

Frederico, L.A., Kunkel, T.A., and Shaw, B.R. (1990). A sensitive genetic assay for the detection of cytosine deamination: determination of rate constants and the activation energy. Biochemistry **29** (10): 2532–2537.

Gall, A.D., Gall, A., Moore, A.C., Aune, M.K., Heid, S., Mori, A., and Burgis, N.E. (2013). Analysis of human ITPase nucleobase specificity by site-directed mutagenesis. Biochimie **95** (9): 1711–1721.

Hadwiger, L.A., and Tanaka, K. (2017). Non-host resistance: DNA damage is associated with sa signaling for induction of pr genes and contributes to the growth suppression of a pea pathogen on pea endocarp tissue. Frontiers in Plant Science **8**: 446.

Haferkamp, I., Fernie, A.R., and Neuhaus, H.E. (2011). Adenine nucleotide transport in plants: much more than a mitochondrial issue. Trends in Plant Science **16** (9): 507–515.

Handley, M.T., Reddy, K., Wills, J., Rosser, E., Kamath, A., Halachev, M., Falkous, G., Williams, D., Cox, P., Meynert, A., Raymond, E.S., Morrison, H., Brown, S., Allan, E., Aligianis, I., Jackson, A.P., Ramsahoye, B.H., Kriegsheim, A. von, **Taylor, R.W., Finch, A.J., and FitzPatrick, D.R.** (2019). ITPase deficiency causes a Martsolf-like syndrome with a lethal infantile dilated cardiomyopathy. PLoS Genetics **15** (3): e1007605.

Hanson, A.D., Henry, C.S., Fiehn, O., and Crécy-Lagard, V. de (2016). Metabolite damage and metabolite damage control in plants. Annual Review of Plant Biology **67**: 131–152.

Harris, C., and Baulcombe, D. (2015). Chlorophyll content assay to quantify the level of necrosis induced by different R gene/elicitor combinations after transient expression. Bio-Protocol **5** (23).

Heinemann, K.J., Yang, S.-Y., Straube, H., Medina-Escobar, N., Varbanova-Herde, M., Herde, M., Rhee, S., and Witte, C.-P. (2021). Initiation of cytosolic plant purine nucleotide catabolism involves a monospecific xanthosine monophosphate phosphatase. Nature communications **12** (1): 6846.

Herberich, E., Sikorski, J., and Hothorn, T. (2010). A robust procedure for comparing multiple means under heteroscedasticity in unbalanced designs. PLoS ONE **5** (3): e9788.

Holmes, S.L., Turner, B.M., and Hirschhorn, K. (1979). Human inosine triphosphatase: Catalytic properties and population studies. Clinica Chimica Acta **97** (2-3): 143–153.

Hooper, C.M., Castleden, I.R., Tanz, S.K., Aryamanesh, N., and Millar, A.H. (2017). SUBA4: the interactive data analysis centre for Arabidopsis subcellular protein locations. Nucleic Acids Research **45** (D1): D1064-D1074.

James, A.M., Seal, S.E., Bailey, A.M., and Foster, G.D. (2021). Viral inosine triphosphatase: A mysterious enzyme with typical activity, but an atypical function. Molecular Plant Pathology **22** (3): 382–389.

Janků, M., Luhová, L., and Petřivalský, M. (2019). On the origin and fate of reactive oxygen species in plant cell compartments. Antioxidants (Basel, Switzerland) **8** (4).

Ji, D., Stepchenkova, E.I., Cui, J., Menezes, M.R., Pavlov, Y.I., and Kool, E.T. (2017). Measuring deaminated nucleotide surveillance enzyme ITPA activity with an ATP-releasing nucleotide chimera. Nucleic Acids Research **45** (20): 11515–11524.

Jiang, H.-P., Xiong, J., Liu, F.-L., Ma, C.-J., Tang, X.-L., Yuan, B.-F., and Feng, Y.-Q. (2018). Modified nucleoside triphosphates exist in mammals. Chemical Science **9** (17): 4160–4167.

Kamiya, H. (2003). Mutagenic potentials of damaged nucleic acids produced by reactive oxygen/nitrogen species: approaches using synthetic oligonucleotides and nucleotides: survey and summary. Nucleic Acids Research **31** (2): 517–531.

Keya, C.A., Crozier, A., and Ashihara, H. (2003). Inhibition of caffeine biosynthesis in tea (Camellia sinensis) and coffee (Coffea arabica) plants by ribavirin. FEBS Letters **554** (3): 473–477.

Klinker, J.F., and Seifert, R. (1997). Functionally nonequivalent interactions of guanosine 5′-triphosphate, inosine 5′-triphosphate, and xanthosine 5′-triphosphate with the retinal G-protein, transducin, and with Gi-proteins in HL-60 leukemia cell membranes. Biochemical Pharmacology **54** (5): 551–562.

Kong, R.P.W., Siu, S.O., Lee, S.S.M., Lo, C., and Chu, I.K. (2011). Development of online high-/low-pH reversed-phase-reversed-phase two-dimensional liquid chromatography for shotgun proteomics: a reversed-phase-strong cation exchange-reversed-phase approach. Journal of Chromatography. A **1218** (23): 3681–3688.

Kumar, S., Stecher, G., Li, M., Knyaz, C., and Tamura, K. (2018). MEGA X: Molecular evolutionary genetics analysis across computing platforms. Molecular Biology and Evolution **35** (6): 1547–1549.

Kuskovsky, R., Buj, R., Xu, P., Hofbauer, S., Doan, M.T., Jiang, H., Bostwick, A., Mesaros, C., Aird, K.M., and Snyder, N.W. (2019). Simultaneous isotope dilution quantification and metabolic tracing of deoxyribonucleotides by liquid chromatography high resolution mass spectrometry. Analytical Biochemistry **568**: 65–72.

Leiva, A.M., Jimenez, J., Sandoval, H., Perez, S., and Cuellar, W.J. (2022). Complete genome sequence of a novel secovirid infecting cassava in the Americas. Archives of Virology.

Lerma-Ortiz, C., Jeffryes, J.G., Cooper, A.J.L., Niehaus, T.D., Thamm, A.M.K., Frelin, O., Aunins, T., Fiehn, O., Crécy-Lagard, V. de, **Henry, C.S., and Hanson, A.D.** (2016). 'Nothing of chemistry disappears in biology': the Top 30 damage-prone endogenous metabolites. Biochemical Society Transactions **44** (3): 961–971.

Li, Z., Kim, J.H., Kim, J., Lyu, J.I., Zhang, Y., Guo, H., Nam, H.G., and Woo, H.R. (2020). ATM suppresses leaf senescence triggered by DNA double-strand break through epigenetic control of senescence-associated genes in Arabidopsis. The New Phytologist **227** (2): 473–484.

Lin, S., McLennan, A.G., Ying, K., Wang, Z., Gu, S., Jin, H., Wu, C., Liu, W., Yuan, Y., Tang, R., Xie, Y., and Mao, Y. (2001). Cloning, expression, and characterization of a human inosine triphosphate pyrophosphatase encoded by the itpa gene. Journal of Biological Chemistry **276** (22): 18695–18701.

Lin, A.-J., Zhang, X.-H., Chen, M.-M., and Cao, Q. (2007). Oxidative stress and DNA damages induced by cadmium accumulation. Journal of Environmental Sciences **19** (5): 596–602.

Lindahl, T. (1993). Instability and decay of the primary structure of DNA. Nature **362** (6422): 709–715.

Lindahl, T., and Nyberg, B. (1974). Heat-induced deamination of cytosine residues in deoxyribonucleic acid. Biochemistry **13** (16): 3405–3410.

Littlejohn, G.R., Gouveia, J.D., Edner, C., Smirnoff, N., and Love, J. (2010). Perfluorodecalin enhances in vivo confocal microscopy resolution of Arabidopsis thaliana mesophyll. The New Phytologist **186** (4): 1018–1025.

Liu, S., Yu, F., Yang, Z., Wang, T., Xiong, H., Chang, C., Yu, W., and Li, N. (2018). Establishment of Dimethyl Labeling-based Quantitative Acetylproteomics in Arabidopsis. Molecular & Cellular Proteomics **17** (5): 1010–1027.

Lu, S., Wang, J., Chitsaz, F., Derbyshire, M.K., Geer, R.C., Gonzales, N.R., Gwadz, M., Hurwitz, D.I., Marchler, G.H., Song, J.S., Thanki, N., Yamashita, R.A., Yang, M., Zhang, D., Zheng, C., Lanczycki, C.J., and Marchler-Bauer, A. (2020). CDD/SPARCLE: the conserved domain database in 2020. Nucleic Acids Research **48** (D1): D265-D268.

Galperin, M. Y., Moroz, O. V., Wilson, K. S., and Murzin, A. G. (2006). House cleaning, a part of good housekeeping. Molecular Microbiology **59** (1): 5–19.

Muraoka, M., Fukuzawa, H., Nishida, A., Okano, K., Tsuchihara, T., Shimoda, A., Suzuki, Y., Sato, M., Osumi, M., and Sakai, H. (1999). The effects of various GTP analogues on microtubule assembly. Cell Structure and Function **24** (2): 101–109.

Myrach, T., Zhu, A., and Witte, C.-P. (2017). The assembly of the plant urease activation complex and the essential role of the urease accessory protein G (UreG) in delivery of nickel to urease. The Journal of Biological Chemistry **292** (35): 14556–14565.

Nagy, G.N., Leveles, I., and Vértessy, B.G. (2014). Preventive DNA repair by sanitizing the cellular (deoxy)nucleoside triphosphate pool. The FEBS journal **281** (18): 4207–4223.

Niehaus, M., Straube, H., Künzler, P., Rugen, N., Hegermann, J., Giavalisco, P., Eubel, H., Witte, C.-P., and Herde, M. (2020). Rapid Affinity Purification of Tagged Plant Mitochondria (Mito-AP) for Metabolome and Proteome Analyses. Plant Physiology **182** (3): 1194–1210.

Niehaus, T.D., Patterson, J.A., Alexander, D.C., Folz, J.S., Pyc, M., MacTavish, B.S., Bruner, S.D., Mullen, R.T., Fiehn, O., and Hanson, A.D. (2019). The metabolite repair enzyme Nit1 is a dual-targeted amidase that disposes of damaged glutathione in Arabidopsis. The Biochemical Journal **476** (4): 683–697.

Niehaus, T.D., Richardson, L.G.L., Gidda, S.K., ElBadawi-Sidhu, M., Meissen, J.K., Mullen, R.T., Fiehn, O., and Hanson, A.D. (2014). Plants utilize a highly conserved system for repair of NADH and NADPH hydrates. Plant Physiology **165** (1): 52–61.

Noskov, V.N., Staak, K., Shcherbakova, P.V., Kozmin, S.G., Negishi, K., Ono, B.-C., Hayatsu, H., and Pavlov, Y.I. (1996). HAM1, the gene controlling 6-N-hydroxylaminopurine sensitivity and mutagenesis in the yeast Saccharomyces cerevisiae. Yeast **12** (1): 17–29.

Fernández-Bautista, N., Domínguez-Núñez, J. A., Moreno, M. M. C., and Berrocal-Lobo, M. (2016). Plant Tissue Trypan Blue Staining During Phytopathogen Infection. Bio-Protocol **6** (24): e2078-e2078.

Oberacker, P., Stepper, P., Bond, D.M., Höhn, S., Focken, J., Meyer, V., Schelle, L., Sugrue, V.J., Jeunen, G.-J., Moser, T., Hore, S.R., Meyenn, F. von, **Hipp, K., Hore, T.A., and Jurkowski, T.P.** (2019). Bio-On-Magnetic-Beads (BOMB): Open platform for high-throughput nucleic acid extraction and manipulation. PLoS Biology **17** (1): e3000107.

Osheroff, N., Shelton, E.R., and Brutlag, D.L. (1983). DNA topoisomerase II from Drosophila melanogaster. Relaxation of supercoiled DNA. Journal of Biological Chemistry **258** (15): 9536–9543.

Pang, B., McFaline, J.L., Burgis, N.E., Dong, M., Taghizadeh, K., Sullivan, M.R., Elmquist, C.E., Cunningham, R.P., and Dedon, P.C. (2012). Defects in purine nucleotide metabolism lead to substantial incorporation of xanthine and hypoxanthine into DNA and RNA. Proceedings of the National Academy of Sciences of the United States of America **109** (7): 2319–2324.

Pétriacq, P., Ton, J., Patrit, O., Tcherkez, G., and Gakière, B. (2016). NAD Acts as an Integral Regulator of Multiple Defense Layers. Plant Physiology **172** (3): 1465–1479.

Pietrowska-Borek, M., Dobrogojski, J., Sobieszczuk-Nowicka, E., and Borek, S. (2020). New Insight into Plant Signaling: Extracellular ATP and Uncommon Nucleotides. Cells **9** (2).

Rampazzo, C., Miazzi, C., Franzolin, E., Pontarin, G., Ferraro, P., Frangini, M., Reichard, P., and Bianchi, V. (2010). Regulation by degradation, a cellular defense against deoxyribonucleotide pool imbalances. Mutation Research **703** (1): 2–10.

Rinne, J., Witte, C.-P., and Herde, M. (2021). Loss of MAR1 Function is a Marker for Co-Selection of CRISPR-Induced Mutations in Plants. Frontiers in Genome Editing **3**: 723384.

Rudd, S.G., Valerie, N.C.K., and Helleday, T. (2016). Pathways controlling dNTP pools to maintain genome stability. DNA Repair **44**: 193–204.

Sakumi, K., Abolhassani, N., Behmanesh, M., Iyama, T., Tsuchimoto, D., and Nakabeppu, Y. (2010). ITPA protein, an enzyme that eliminates deaminated purine nucleoside triphosphates in cells. Mutation Research **703** (1): 43–50.

Savchenko, A., Proudfoot, M., Skarina, T., Singer, A., Litvinova, O., Sanishvili, R., Brown, G., Chirgadze, N., and Yakunin, A.F. (2007). Molecular basis of the antimutagenic activity of the house-cleaning inosine triphosphate pyrophosphatase RdgB from Escherichia coli. Journal of Molecular Biology **374** (4): 1091–1103.

Simone, P.D., Pavlov, Y.I., and Borgstahl, G.E.O. (2013). ITPA (inosine triphosphate pyrophosphatase): from surveillance of nucleotide pools to human disease and pharmacogenetics. Mutation Research **753** (2): 131–146.

Spee, J.H., Vos, W.M. de, and **Kuipers, O.P.** (1993). Efficient random mutagenesis method with adjustable mutation frequency by use of PCR and dITP. Nucleic Acids Research **21** (3): 777–778.

Stenmark, P., Kursula, P., Flodin, S., Gräslund, S., Landry, R., Nordlund, P., and Schüler, H. (2007). Crystal structure of human inosine triphosphatase. Substrate binding and implication of the inosine triphosphatase deficiency mutation P32T. Journal of Biological Chemistry **282** (5): 3182–3187.

Straube, H., Niehaus, M., Zwittian, S., Witte, C.-P., and Herde, M. (2020). Enhanced nucleotide analysis enables the quantification of deoxynucleotides in plants and algae revealing connections between nucleoside and deoxynucleoside metabolism. The Plant Cell.

Thomas, M.J., Platas, A.A., and Hawley, D.K. (1998). Transcriptional Fidelity and Proofreading by RNA Polymerase II. Cell **93** (4): 627–637.

Tian, T., Liu, Y., Yan, H., You, Q., Yi, X., Du, Z., Xu, W., and Su, Z. (2017). agriGO v2.0: a GO analysis toolkit for the agricultural community, 2017 update. Nucleic Acids Research **45** (W1): W122-W129.

Tomlinson, K.R., Pablo-Rodriguez, J.L., Bunawan, H., Nanyiti, S., Green, P., Miller, J., Alicai, T., Seal, S.E., Bailey, A.M., and Foster, G.D. (2019). Cassava brown streak virus Ham1 protein hydrolyses mutagenic nucleotides and is a necrosis determinant. Molecular Plant Pathology **20** (8): 1080–1092.

Traube, F. R., Schiffers, S., Iwan, K., Kellner, S., Spada, F., Müller, M., and Carell, T. (2019). Isotope-dilution mass spectrometry for exact quantification of noncanonical DNA nucleosides. Nature Protocols **14** (1): 283–312.

Tripathi, D., Nam, A., Oldenburg, D.J., and Bendich, A.J. (2020). Reactive Oxygen Species, Antioxidant Agents, and DNA Damage in Developing Maize Mitochondria and Plastids. Frontiers in Plant Science **11**: 596.

Valderrama, R., Corpas, F.J., Carreras, A., Fernández-Ocaña, A., Chaki, M., Luque, F., Gómez-Rodríguez, M.V., Colmenero-Varea, P., Del Río, L.A., and Barroso, J.B. (2007). Nitrosative stress in plants. FEBS Letters **581** (3): 453–461.

Vanderheiden, B.S. (1969). Genetic studies of human erythrocyte inosine triphosphatase. Biochemical Genetics **3** (3): 289–297.

Vanderheiden, B.S. (1979). Possible implication of an inosinetriphosphate metabolic error and glutamic acid decarboxylase in paranoid schizophrenia. Biochemical Medicine **21** (1): 22–32.

Wang, C., and Liu, Z. (2006). Arabidopsis ribonucleotide reductases are critical for cell cycle progression, DNA damage repair, and plant development. The Plant Cell **18** (2): 350–365.

Wang, Z.-P., Xing, H.-L., Dong, L., Zhang, H.-Y., Han, C.-Y., Wang, X.-C., and Chen, Q.-J. (2015). Egg cell-specific promoter-controlled CRISPR/Cas9 efficiently generates homozygous mutants for multiple target genes in Arabidopsis in a single generation. Genome Biology **16**: 144.

Weber, J., and Senior, A.E. (2001). Bi-site catalysis in F1-ATPase: does it exist? Journal of Biological Chemistry **276** (38): 35422–35428.

Witte, C.-P., and Herde, M. (2020). Nucleotide Metabolism in Plants. Plant Physiology **182** (1): 63–78.

Witte, C.-P., Rosso, M.G., and Romeis, T. (2005). Identification of three urease accessory proteins that are required for urease activation in Arabidopsis. Plant Physiology **139** (3): 1155–1162.

Yan, S., Wang, W., Marqués, J., Mohan, R., Saleh, A., Durrant, W.E., Song, J., and Dong, X. (2013). Salicylic acid activates DNA damage responses to potentiate plant immunity. Molecular Cell **52** (4): 602–610.

Yang, Z.-B., He, C., Ma, Y., Herde, M., and Ding, Z. (2017). Jasmonic Acid Enhances Al-Induced Root Growth Inhibition. Plant Physiology **173** (2): 1420–1433.

Yoneshima, Y., Abolhassani, N., Iyama, T., Sakumi, K., Shiomi, N., Mori, M., Shiomi, T., Noda, T., Tsuchimoto, D., and Nakabeppu, Y. (2016). Deoxyinosine triphosphate induces MLH1/PMS2- and p53-dependent cell growth arrest and DNA instability in mammalian cells. Scientific Reports **6**: 32849.

Yoshimura, K., Ogawa, T., Ueda, Y., and Shigeoka, S. (2007). AtNUDX1, an 8-oxo-7,8-dihydro-2'-deoxyguanosine 5'-triphosphate pyrophosphohydrolase, is responsible

for eliminating oxidized nucleotides in Arabidopsis. Plant & Cell Physiology **48** (10): 1438–1449.

Yu, D., Song, W., Tan, E.Y.J., Liu, L., Cao, Y., Jirschitzka, J., Li, E., Logemann, E., Xu, C., Huang, S., Jia, A., Chang, X., Han, Z., Wu, B., Schulze-Lefert, P., and Chai, J. (2021). TIR domains of plant immune receptors are 2′,3′-cAMP/cGMP synthetases mediating cell death. bioRxiv

FIGURE LEGENDS

Figure 1. Phylogenetic analysis of ITPA in several organisms

An unrooted maximum likelihood tree was build using MEGAX, comprising model species from a wide taxonomic range. The tree with the best log-score is shown with branch length indicating the number of site-substitutions (scale-bar). Numbers at branches indicate the percentage of trees in which associated taxa clustered together in the bootstrap analysis (1000 bootstraps). Values below 80 are not shown. Species name abbreviations are listed in the legend of Supplemental Figure 2.

Figure 2. Characterization of the enzymatic properties of ITPA

(A) Reaction scheme of ITPA with ITP. (B) Affinity purified, C-terminal Strep-tagged ITPA on a Coomassie stained gel (left) and detection of ITPA by immunoblotting using an antibody against the Strep-tag (right). Numbers indicate the respective size in kilodalton (kDa). crude, centrifuged extract; unbound, centrifuged extract after incubation with Strep-tactin matrix; 5th wash, supernatant after the fifth wash of the affinity matrix; elution, eluate of the affinity matrix; boil off, supernatant after boiling the affinity matrix in SDS loading buffer. (C) Specific activity of ITPA with different substrate at a concentration of 200 µM. (D) Determination of kinetic constants for the ITPA catalyzed reaction of dITP to dIMP. Kinetic data was fitted using the Michaelis-Menten equation (orange) or by linear regression for the Hanes plot (S/V, purple). Error bars are SD, n = 3 reactions. S, substrate concentration; V, enzymatic activity. (E) The same as in (D), but using ITP as substrate.

Figure 3. Characterization of *itpa* mutant lines

(A) Organization of the At4g13720 locus encoding ITPA and positions of T-DNA insertion sites (SALK053023; Δ *itpa-1*), as well as binding site of the guide RNAs

(gRNAs) used to generate Δ *itpa-2*. The respective gRNAs are shown below as well as the single base pair insertions observed in *itpa-2*. Exons are shown as green blocks, introns as white blocks. Arrows indicate primer positions. (B) PCR-analysis of the wildtype and *itpa-1* alleles (left panel), as well as RT-PCRs to assess the presence of intact mRNA in homozygous *itpa-1* lines (right panel) and the corresponding wildtype selected from a segregating mutant population. The mRNA of the actin2 gene (At3g18780) was amplified as control.

Figure 4. Phenotypic comparison of wild type, *itpa-1* and *itpa-2* plants

(A) Rosette leaves of 40-day-old wild type, *itpa-1* and *itpa-2* plants grown under long day conditions. Bars = 10 mm. (B) Representative picture of the oldest leaves from 56-day-old plants of different genotypes used in (C). (C) Chlorophyll content of the respective oldest leaves from 56-day-old plants of different genotypes. n = 5, every replicate represents a different plant of the same genotype. (D) Leaves of 56-days-old wild type, *itpa-1* and *itpa-2* plants were stained by trypan blue and dark pixels per leaf-area were measured using ImageJ. Error bars are SD, n = 4 - 5. Statistical analysis was performed by a two-sided Tukey's pairwise comparison using the sandwich variance estimator. Different letters indicate p values < 0.05. All p values can be found in the Supplemental Table 1.

Figure 5. Subcellular localization of ITPA

(A) Confocal fluorescence microscopy images of leaf epidermal cells of two-weeks-old, stable transformed *itpa-2* mutant plants expressing ITPA C-terminally fused to YFP. Left panel, YFP fluorescence; middle panel, chloroplast auto fluorescence; right panel, overlay of both. (B) The same as in (A) but in roots. Bars = 10 µm.

Figure 6. Loss of function of *itpa* causes an accumulation of IDP and ITP while adenylate concentrations remain unchanged.

(A) Concentrations of inosylates in rosette leaves of 35-day-old wild type, *itpa-1* and *itpa-2* plants. (B) As in (A) but for ADP and ATP. Error bars are SD, n = 6, every replicate represents a different plant. Statistical analysis was performed by a two-sided Tukey's pairwise comparison using the sandwich variance estimator. Different letters

indicate *p* values < 0.05. All *p* values can be found in the Supplemental Table 1. n.d. = not detected.

Figure 7. Concentrations of different nucleotides in untreated and CBSV- infected *N. benthamiana* plants.

(A) Adult plants of *N. benthamiana* were mock treated (untreated) or infected with cassava brown streak virus (CBSV). The youngest, systemically infected leaves were harvested after 21 days. Concentrations of inosylates are shown. Error bars are SD, *n* = 3. (B) Same as in (A) but canonical ribonucleotide triphosphates are shown. Statistical analysis was performed by a two-sided Tukey's pairwise comparison using the sandwich variance estimator. Different letters indicate *p* values < 0.05. All *p* values can be found in the Supplemental Table 1.

Figure 8. Manipulation of IMP content in leaves of *N. benthamiana* does not alter ITP concentrations.

IMP (upper panel) and ITP (lower panel) in leaves of 21-day-old *N. benthamiana* plants. The leaves were either not treated or mock infiltrated with buffer on one leaf or infiltrated with buffer containing ribavirin (500 µM) on the opposite leaf. Error bars are SD, *n* = 5, every replicate representing a leaf from an independent plant. Statistical analysis was performed by a two-sided Tukey's pairwise comparison using the sandwich variance estimator. Different letters indicate *p* values < 0.05. All *p* values can be found in the Supplemental Table 1.

Figure 9. Enzymatic activity of AMPK 3 and 4 with AMP and IMP

Enzymes were transiently expressed in *N. benthamiana* as C-terminal Strep-tagged variants and affinity purified. (A) Specific activity of AMPK3 with 1 mM AMP or IMP in the presence of 1 mM ATP. Linear rates were observed in all cases. Error bars are SD. Each replicate represents an independent enzyme assay from the same enzyme preparation (*n* = 4). (B) Analogous data for AMPK4.

Figure 10. The effect of cadmium causing oxidative stress on inosylate concentrations.

Mutant and wild type plants grown in a hydroponic system for 14 days were treated with 10 µM cadmium sulfate for 24 h or were left untreated. ITP, IDP and IMP were quantified. Error bars are SD, *n* = 4, every replicate represents a pool of plants from an independent hydroponic vessel. Statistical analysis was performed by a two-sided Tukey's pairwise comparison using the sandwich variance estimator. Different letters indicate *p* values < 0.05. All *p* values can be found in the Supplemental Table 1. n.d. = not detected.

Figure 11. Concentration of deoxyinosine and inosine in nucleic acids of different genotypes.

(A) Molecules of deoxyinosine per million molecules of deoxyadenosine in DNA isolated from pools of 7-day-old Arabidopsis seedlings grown on agar plates and 56-day-old Arabidopsis rosettes. Error bars are SD, *n* = 5 and 3. (B) Molecules of inosine per million molecules adenosine in total RNA isolated from 35-day-old Arabidopsis rosettes. Error bars are SD, *n* = 5. Every replicate represents a different plant. Statistical analysis was performed by a two-sided Tukey's pairwise comparison using the sandwich variance estimator. Different letters indicate *p* values < 0.05. All *p* values can be found in the Supplemental Table 1. n.d. = not detected.

Figure 12. Overview of deaminated purine nucleotide metabolism and its interplay with purine *de novo* synthesis. Enzymatic and non-enzymatic steps that lead to the generation of deaminated purine nucleotides are shown, as well as their removal by the inosine triphosphate pyrophosphatase (ITPA) and reintegration into canonical purine nucleotide metabolism or potential incorporation into nucleic acids. (d)ATP, (deoxy)adenosine triphosphate; (d)ITP, (deoxy)inosine triphosphate; (d)XTP, (deoxy)xanthosine triphosphate; (d)GTP, (deoxy)guanosine triphosphate; AMP, adenosine monophosphate; (d)IMP, (deoxy)inosine monophosphate; (d)XMP, (deoxy)xanthosine monophosphate; IMPDH, inosine monophosphate dehydrogenase; XMPP, xanthosine monophosphate phosphatase.

Figure 13. Loss-of-function of ITPA leads to differential upregulation of transcripts associated with salicylic acid, systemic acquired resistance as well as aging and increased endogenous concentrations of salicylic acid.

(A) RNA was isolated from 35-day-old Arabidopsis rosettes and analyzed by RNAseq. Log_2 (RPKM) values are shown for genes associated with response to salicylic acid (GO:0009751) and differentially regulated between wild type and *itpa-1* samples. Error bars are SD, *n* = 3. Every replicate represents a pool of two different plants. (B) As in (A) but for genes associated with systemic acquired resistance (GO:0009627). (C) As in (A) but for genes associated with aging (GO:0007568). (D) Concentrations of salicylic acid in 35-day-old Arabidopsis rosettes analyzed by LC-MS. Error bars are SD, *n* = 4. Every replicate represents a different plant. Statistical analysis was performed by a two-sided Tukey's pairwise comparison using the sandwich variance estimator. Different letters indicate *p* values < 0.05. All *p* values can be found in the Supplemental Table 1.

TABLES

Table 1: Comparison of kinetic parameters of plant, fungi and mammal ITPA enzymes

	ITPA (*A. thaliana*; this study)			HAM1 (*S.cervisisiae*; Davies et al., 2011)			ITPA (*H. sapiens; Lin et al., 2001)*		
substrate	K_M	k_{cat}	k_{cat}/K_M	K_M	k_{cat}	k_{cat}/K_M	K_M	k_{cat}	k_{cat}/K_M
	μM	s^{-1}	$mM^{-1}\ s^{-1}$	*μM*	s^{-1}	$mM^{-1}\ s^{-1}$	*μM*	s^{-1}	$mM^{-1}\ s^{-1}$
dITP	1.7 ± 0.3	1.5 ± 0.17	8.8×10^5	3.06 ± 0.6	1.3	4.21×10^5	450 ± 100	360	1.16×10^6
ITP	7.1 ± 1.2	1.9 ± 0.25	2.6×10^5	2.38 ± 0.4	1.0	4.17×10^5	510 ± 100	580	1.14×10^6

Table 2: Ratios of ITP and IDP per million molecules of ATP and ADP, respectively

	itpa-1	***itpa-2***
ITP/ 1×10^6 ATP	36.6 ± 12	28,7 ± 11

IDP/ 1 x 10^6 ADP	300,8 ± 162	407,5 ± 178

Table 3: Precursor ions, transitions (quantifier, qualifier), fragmentor energy and collision energy for dITP, IDP, ITP, XMP and XTP

	Precursor Ion $[M+H]^+$ (m/z)	Product Ion (m/z)	Fragmentor	Collision Energy (V)
dITP	492.99	217	115	10
		137		30
		81.1		30
IDP	429	137	80	10
		97		22
ITP	508.99	137	120	30
		97.1		30
XMP	365.05	212.9	84	3
		153		15
		97.1		17
XTP	525	244.3	17	40
		97		40

Table 4: Precursor ions, transitions (quantifier, qualifier), fragmentor energy and collision energy for phytohormones and the respective deuterated isotope standards

	Precursor Ion $[M-H]^-$ (m/z)	Product Ion (m/z)	Fragmentor	Collision Energy (V)
Absicic acid	263.1	219.1	100	10
		153.1		6
Absicic acid, D6	269.1	225.1	100	10
		159.1		6
Jasmonic acid	209.1	59.1	119	10

Jasmonic acid, D6	215.2	97.1	119	10
Jasmonic acid-Ile	322.2	130	150	18
Jasmonic acid-Ile, D6	328.2	130	150	18
Salicylic acid	137	93	92	14
Salicylic acid, D4	141.1	97.1	92	14

Table 5: Sequencing and mapping results for RNAseq analysis

Sample	**Number of reads**	**Q30 (%)**	**GC (%)**	**Number of mapped reads**	**Number of mapped reads in pairs**
wild type-1	121076316	94.5	46.5	118548394	116476958
wild type-2	135505128	94.6	46.6	133098104	130824630
wild type-3	125869530	93.9	46.5	123590003	121310110
itpa-1.1	123543150	94.7	46.4	120859536	118841618
itpa-1.2	124078898	94.3	46.6	120519925	118410338
itpa-1.3	132188126	94.3	46.1	129656012	127351422

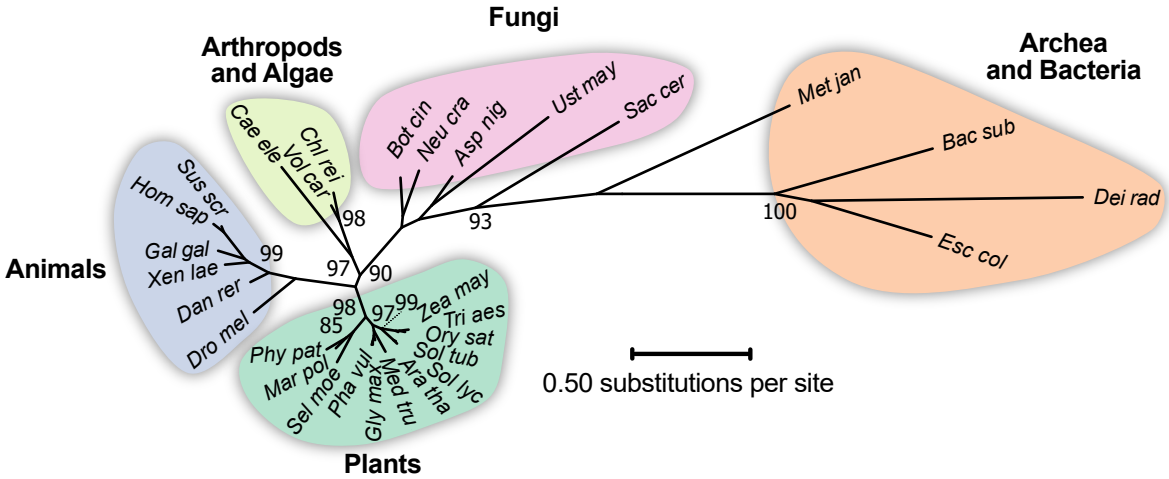

Figure 1. Phylogenetic analysis of ITPA in several organisms

An unrooted maximum likelihood tree was build using MEGAX, comprising model species from a wide taxonomic range. The tree with the best log-score is shown with branch length indicating the number of site-substitutions (scale-bar). Numbers at branches indicate the percentage of trees in which associated taxa clustered together in the bootstrap analysis (1000 bootstraps). Values below 80 are not shown. Species name abbreviations are listed in the legend of Supplemental Figure 2.

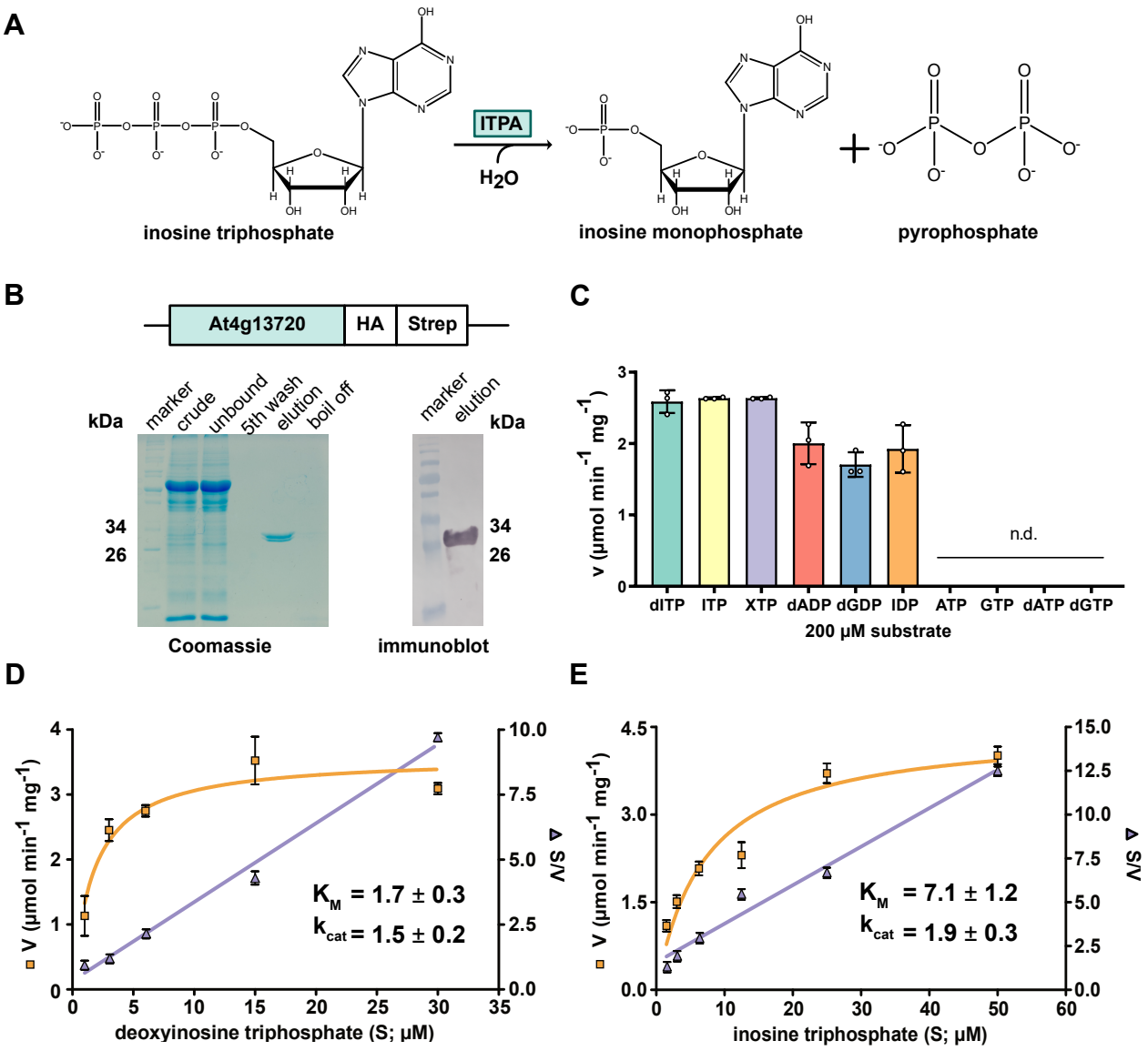

Figure 2. Characterization of the enzymatic properties of ITPA

(A) Reaction scheme of ITPA with ITP. (B) Affinity purified, C-terminal Strep-tagged ITPA on a Coomassie stained gel (left) and detection of ITPA by immunoblotting using an antibody against the Strep-tag (right). Numbers indicate the respective size in kilodalton (kDa). crude, centrifuged extract; unbound, centrifuged extract after incubation with Strep-tactin matrix; 5th wash, supernatant after the fifth wash of the affinity matrix; elution, eluate of the affinity matrix; boil off, supernatant after boiling the affinity matrix in SDS loading buffer. (C) Specific activity of ITPA with different substrate at a concentration of 200 µM. (D) Determination of kinetic constants for the ITPA catalyzed reaction of dITP to dIMP. Kinetic data was fitted using the Michaelis-Menten equation (orange) or by linear regression for the Hanes plot (S/V, purple). Error bars are SD, n = 3 reactions. S, substrate concentration; V, enzymatic activity. (E) The same as in (D), but using ITP as substrate.

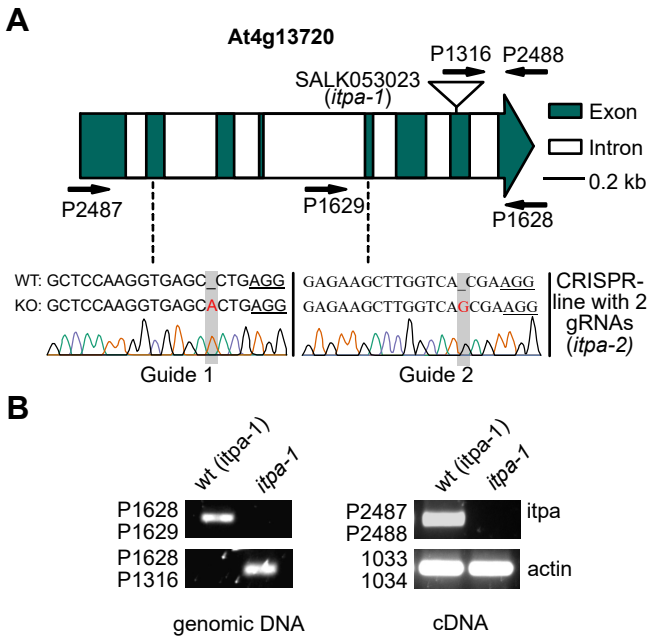

Figure 3. Characterization of *itpa* mutant lines

(A) Organization of the At4g13720 locus encoding ITPA and positions of T-DNA insertion sites (SALK053023; Δ *itpa-1*), as well as binding site of the guide RNAs (gRNAs) used to generate Δ *itpa-2*. The respective gRNAs are shown below as well as the single base pair insertions observed in *itpa-2*. Exons are shown as green blocks, introns as white blocks. Arrows indicate primer positions. (B) PCR-analysis of the wildtype and *itpa-1* alleles (left panel), as well as RT-PCRs to assess the presence of intact mRNA in homozygous *itpa-1* lines (right panel) and the corresponding wildtype selected from a segregating mutant population. The mRNA of the actin2 gene (At3g18780) was amplified as control.

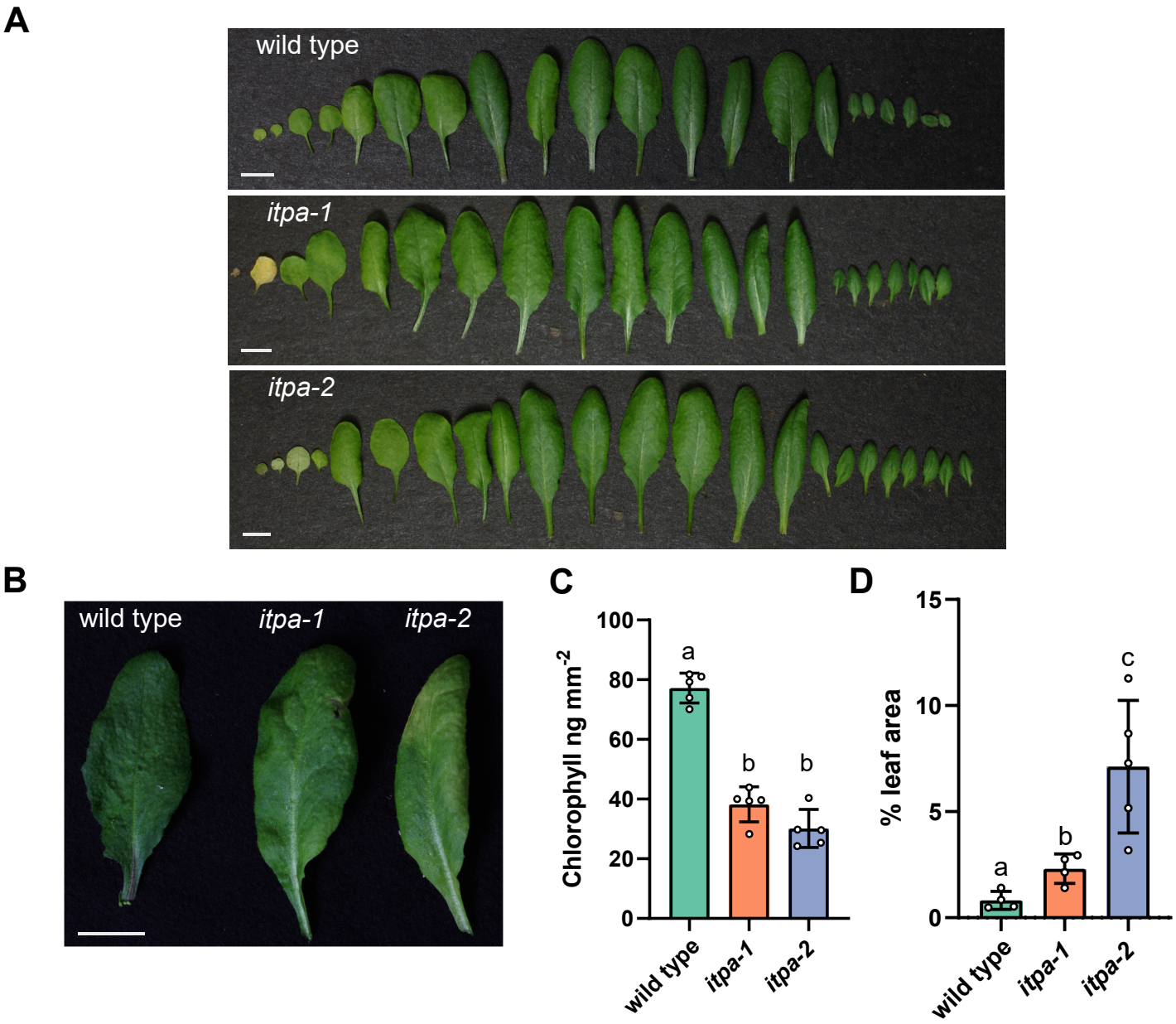

Figure 4. Phenotypic comparison of wild type, *itpa-1* and *itpa-2* plants

(A) Rosette leaves of 40-day-old wild type, *itpa-1* and *itpa-2* plants grown under long day conditions. Bars = 10 mm. (B) Representative picture of the oldest leaves from 56-day-old plants of different genotypes used in (C). (C) Chlorophyll content of the respective oldest leaves from 56-day-old plants of different genotypes. n = 5, every replicate represents a different plant of the same genotype. (D) Leaves of 56-days-old wild type, *itpa-1* and *itpa-2* plants were stained by trypan blue and dark pixels per leaf-area were measured using ImageJ. Error bars are SD, n = 4 - 5. Statistical analysis was performed by a two-sided Tukey's pairwise comparison using the sandwich variance estimator. Different letters indicate p values < 0.05. All p values can be found in the Supplemental Table 1.

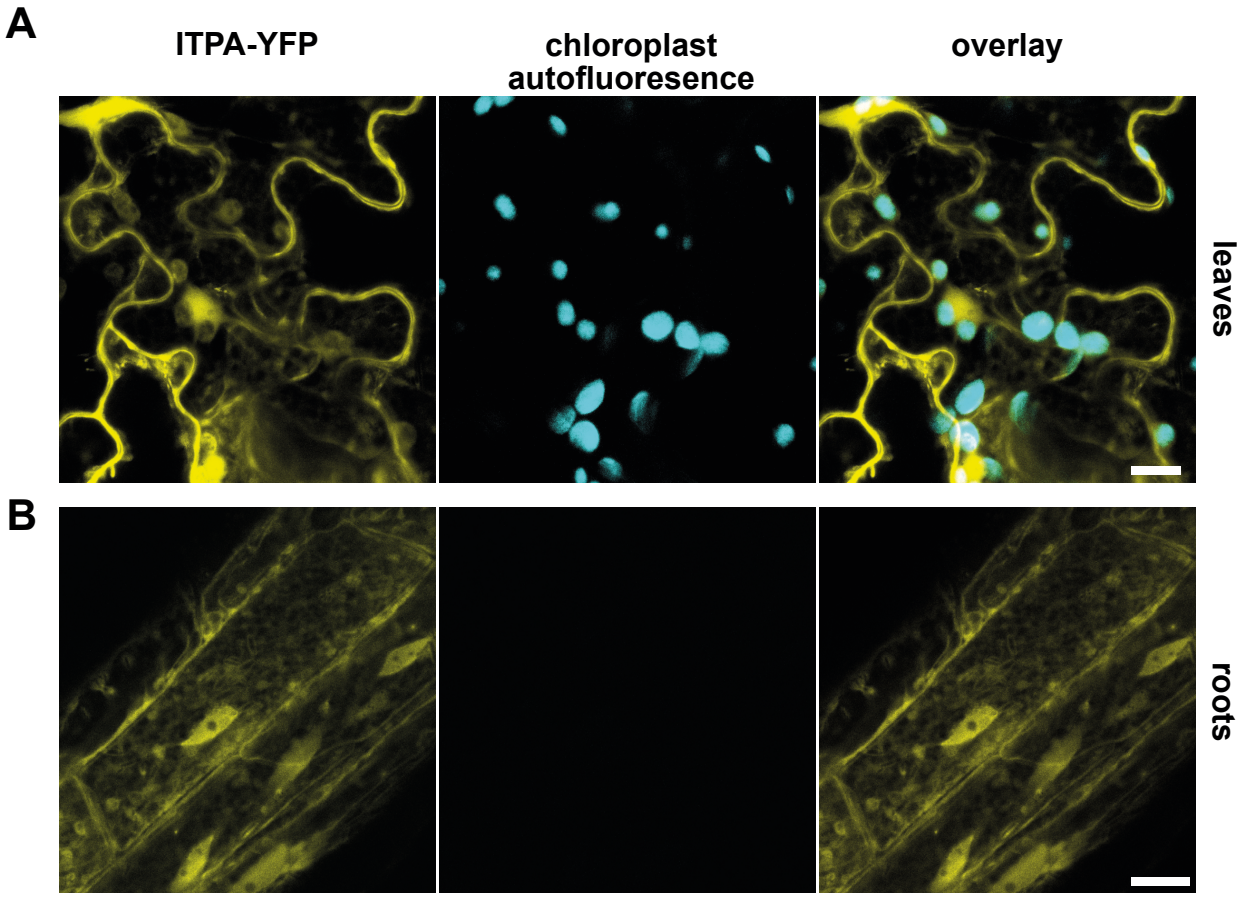

Figure 5. Subcellular localization of ITPA

(A) Confocal fluorescence microscopy images of leaf epidermal cells of two-weeks-old, stable transformed *itpa-2* mutant plants expressing ITPA C-terminally fused to YFP. Left panel, YFP fluorescence; middle panel, chloroplast auto fluorescence; right panel, overlay of both. (B) The same as in (A) but in roots. Bars = 10 µm.

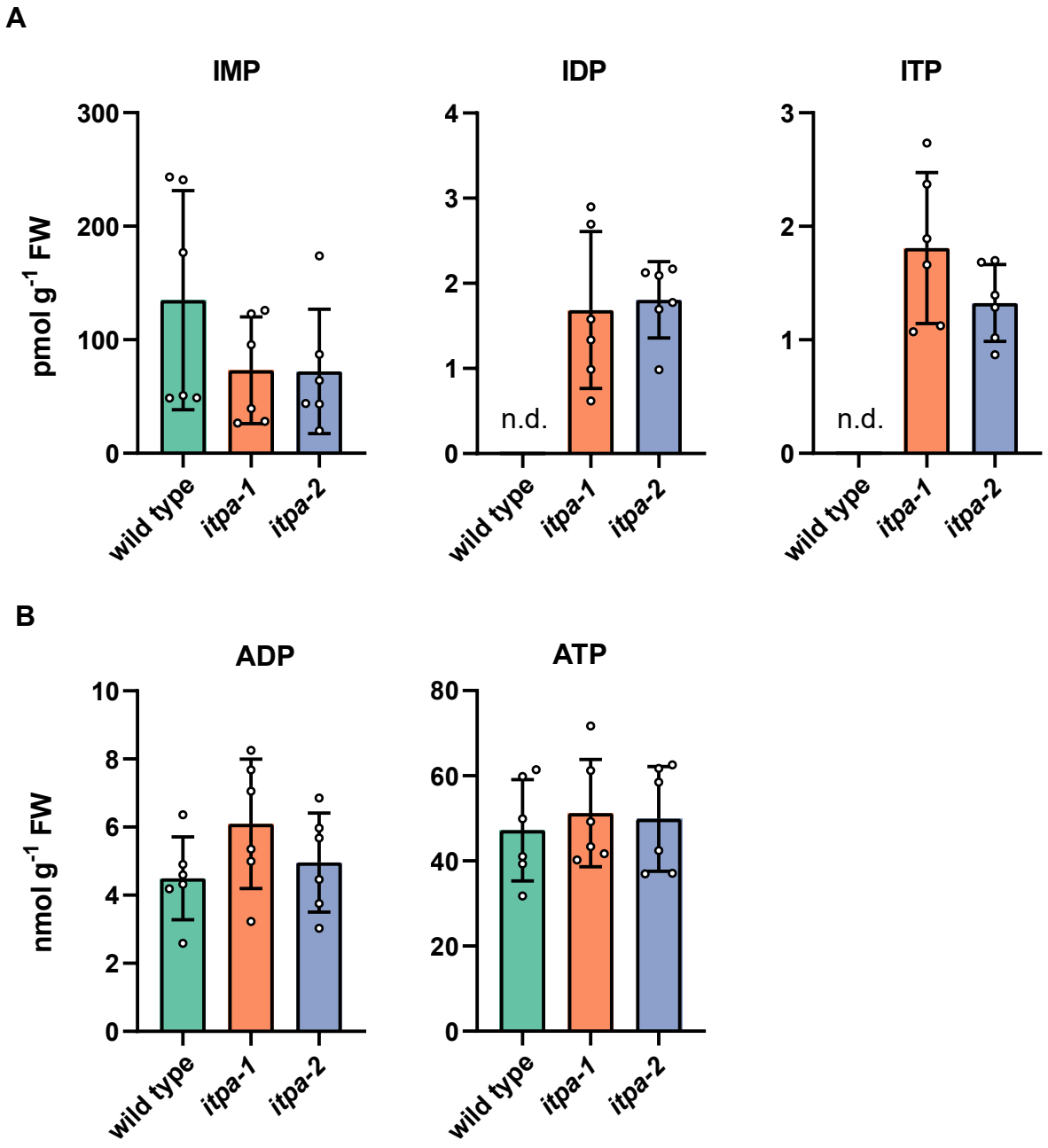

Figure 6. Loss of function of *itpa* causes an accumulation of IDP and ITP while adenylate concentrations remain unchanged.

(A) Concentrations of inosylates in rosette leaves of 35-day-old wild type, *itpa-1* and *itpa-2* plants. (B) As in (A) but for ADP and ATP. Error bars are SD, $n = 6$, every replicate represents a different plant. Statistical analysis was performed by a two-sided Tukey's pairwise comparison using the sandwich variance estimator. Different letters indicate p values < 0.05. All p values can be found in the Supplemental Table 1. n.d. = not detected.

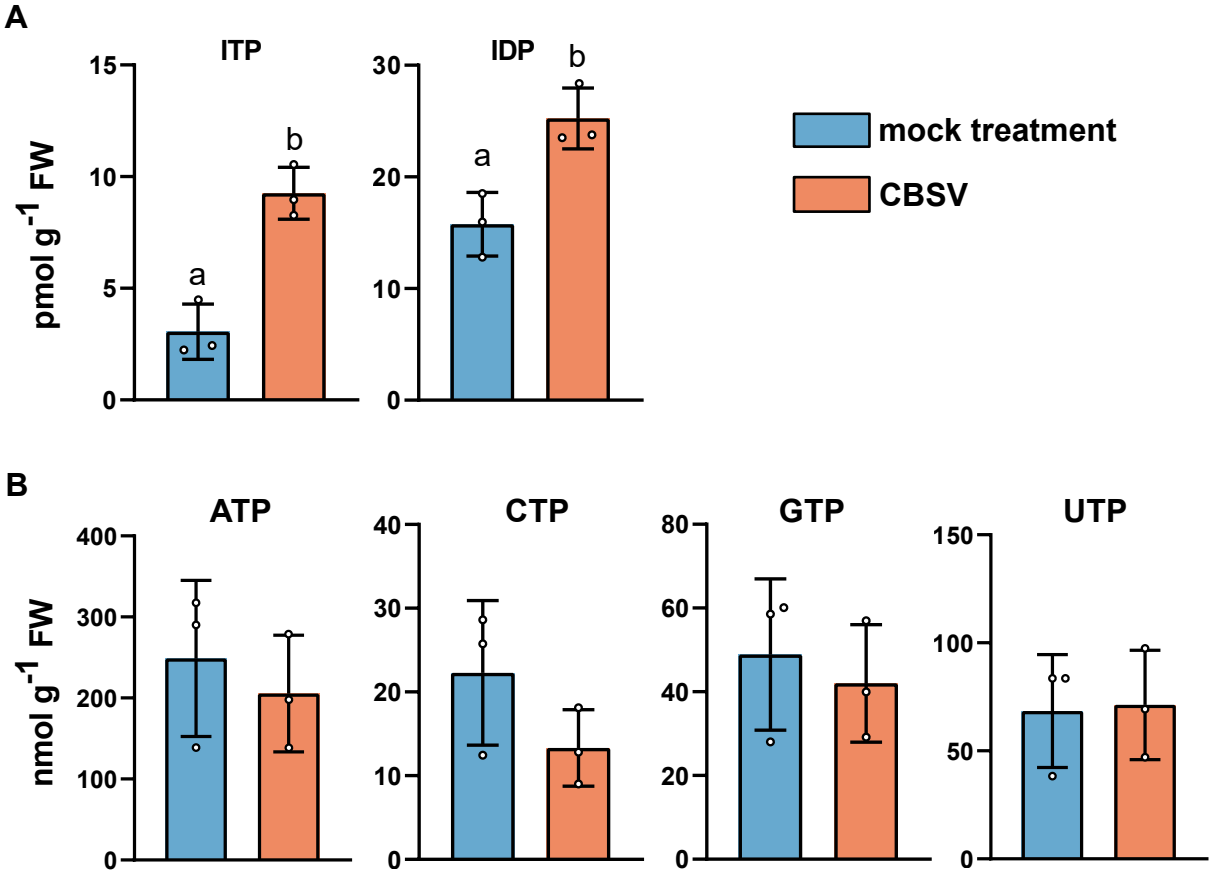

Figure 7. Concentrations of different nucleotides in untreated and CBSV- infected *N. benthamiana* plants.

(A) Adult plants of *N. benthamiana* were mock treated (untreated) or infected with cassava brown streak virus (CBSV). The youngest, systemically infected leaves were harvested after 21 days. Concentrations of inosylates are shown. Error bars are SD, $n = 3$. (B) Same as in (A) but canonical ribonucleotide triphosphates are shown. Statistical analysis was performed by a two-sided Tukey's pairwise comparison using the sandwich variance estimator. Different letters indicate p values < 0.05. All p values can be found in the Supplemental Table 1.

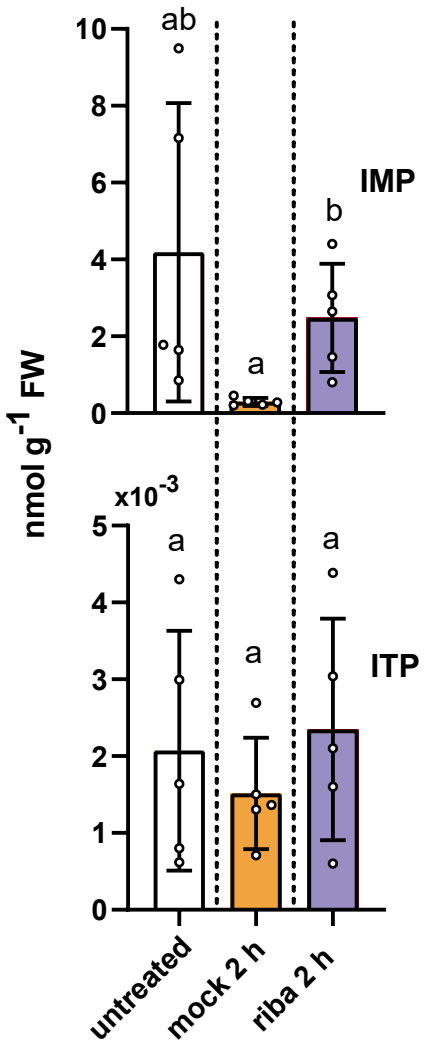

Figure 8. Manipulation of IMP content in leaves of *N. benthamiana* does not alter ITP concentrations.

IMP (upper panel) and ITP (lower panel) in leaves of 21-day-old *N. benthamiana* plants. The leaves were either not treated or mock infiltrated with buffer on one leaf or infiltrated with buffer containing ribavirin (500 µM) on the opposite leaf. Error bars are SD, n = 5, every replicate representing a leaf from an independent plant. Statistical analysis was performed by a two-sided Tukey's pairwise comparison using the sandwich variance estimator. Different letters indicate p values < 0.05. All p values can be found in the Supplemental Table 1.

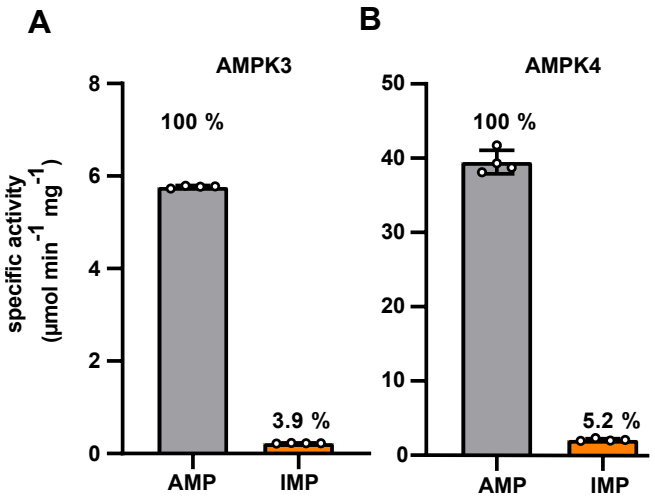

Figure 9. Enzymatic activity of AMPK 3 and 4 with AMP and IMP

Enzymes were transiently expressed in *N. benthamiana* as C-terminal Strep-tagged variants and affinity purified. (A) Specific activity of AMPK3 with 1 mM AMP or IMP in the presence of 1 mM ATP. Linear rates were observed in all cases. Error bars are SD. Each replicate represents an independent enzyme assay from the same enzyme preparation (n = 4). (B) Analogous data for AMPK4.

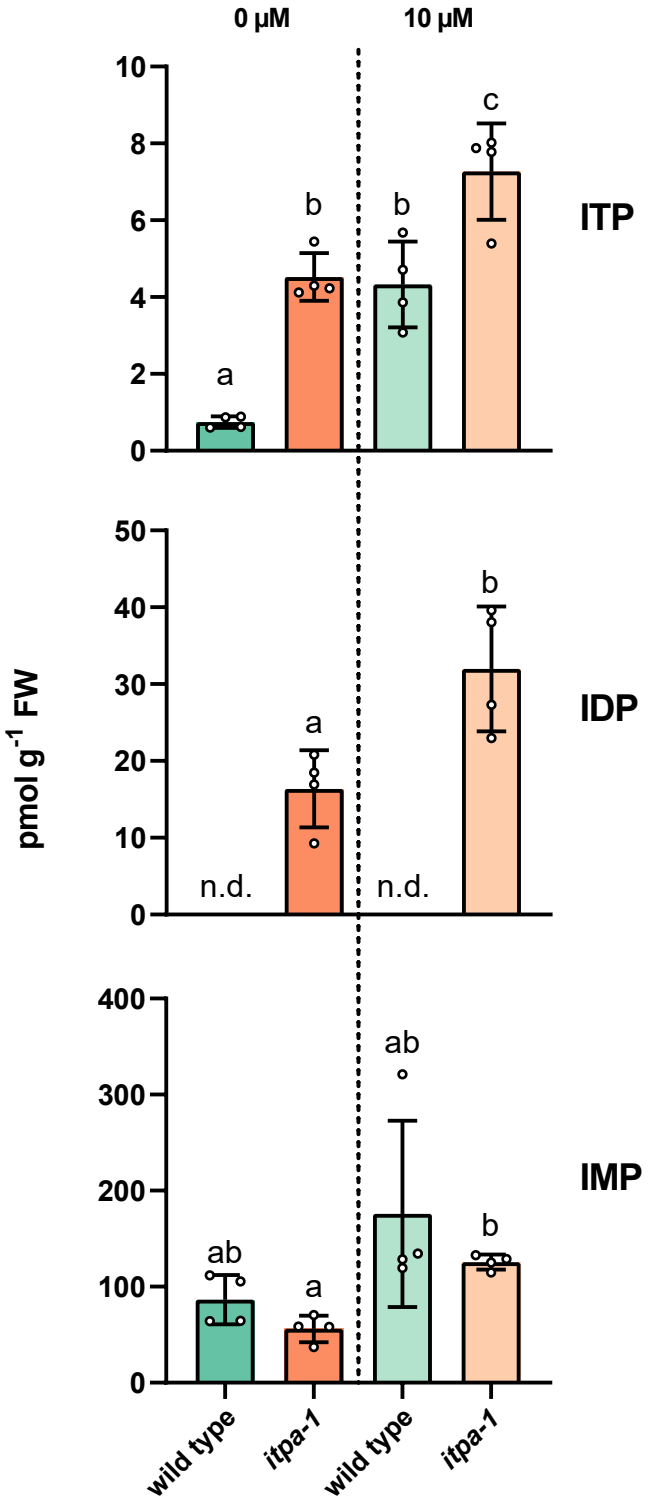

Figure 10. The effect of cadmium causing oxidative stress on inosylate concentrations.

Mutant and wild type plants grown in a hydroponic system for 14 days were treated with 10 µM cadmium sulfate for 24 h or were left untreated. ITP, IDP and IMP were quantified. Error bars are SD, n = 4, every replicate represents a pool of plants from an independent hydroponic vessel. Statistical analysis was performed by a two-sided Tukey's pairwise comparison using the sandwich variance estimator. Different letters indicate p values < 0.05. All p values can be found in the Supplemental Table 1. n.d. = not detected.

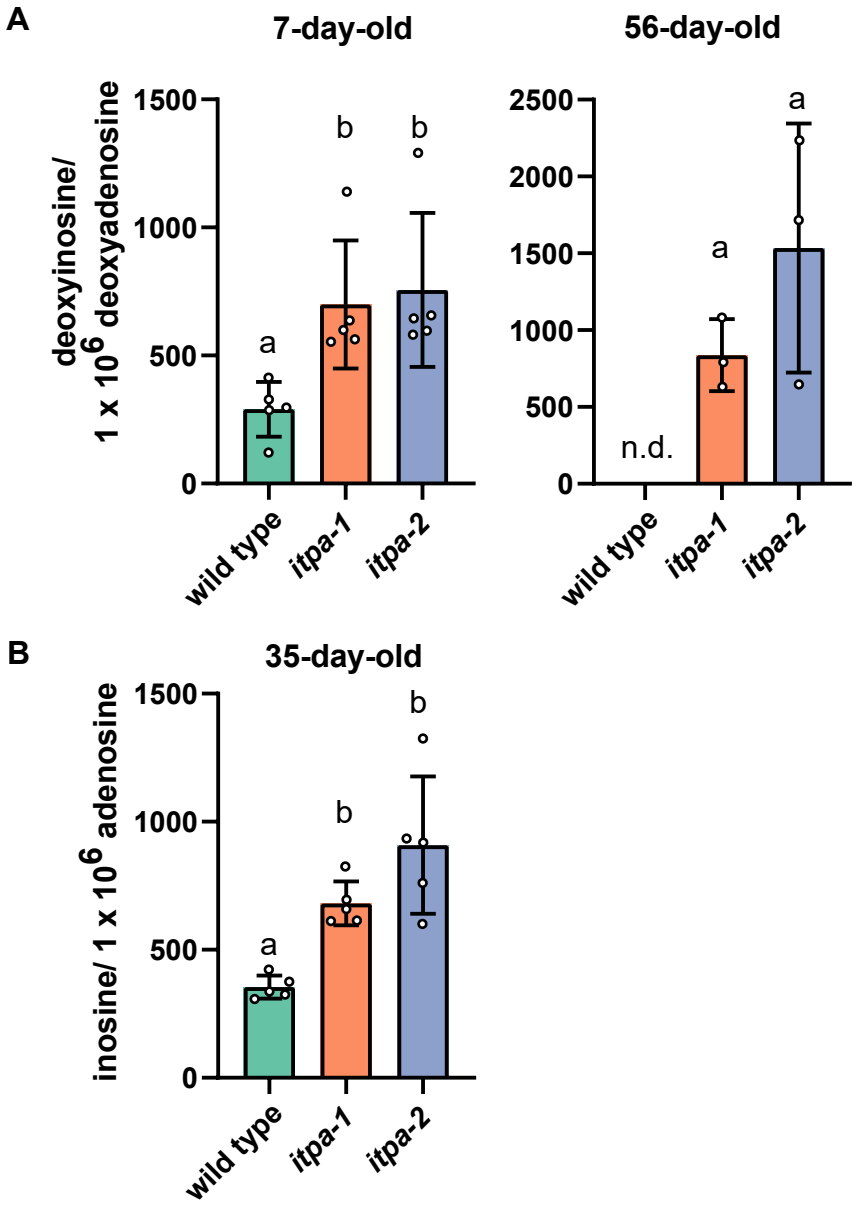

Figure 11. Concentration of deoxyinosine and inosine in nucleic acids of different genotypes.

(A) Molecules of deoxyinosine per million molecules of deoxyadenosine in DNA isolated from pools of 7-day-old Arabidopsis seedlings grown on agar plates and 56-day-old Arabidopsis rosettes. Error bars are SD, n = 5 and 3. (B) Molecules of inosine per million molecules adenosine in total RNA isolated from 35-day-old Arabidopsis rosettes. Error bars are SD, n = 5. Every replicate represents a different plant. Statistical analysis was performed by a two-sided Tukey's pairwise comparison using the sandwich variance estimator. Different letters indicate p values < 0.05. All p values can be found in the Supplemental Table 1. n.d. = not detected

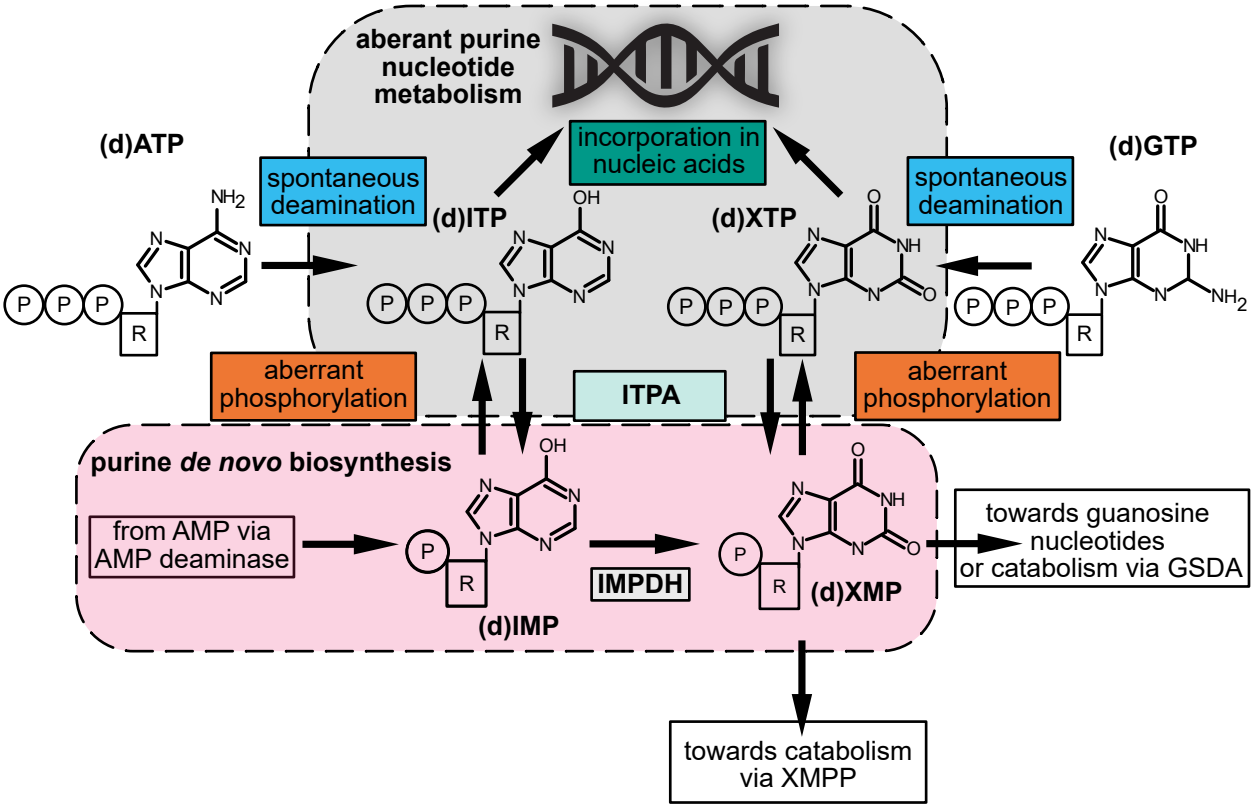

Figure 12. Overview of deaminated purine nucleotide metabolism and its interplay with purine *de novo* synthesis. Enzymatic and non-enzymatic steps that lead to the generation of deaminated purine nucleotides are shown, as well as their removal by the inosine triphosphate pyrophosphatase (ITPA) and reintegration into canonical purine nucleotide metabolism or potential incorporation into nucleic acids. (d)ATP, (deoxy)adenosine triphosphate; (d)ITP, (deoxy)inosine triphosphate; (d)XTP, (deoxy)xanthosine triphosphate; (d)GTP, (deoxy)guanosine triphosphate; AMP, adenosine monophosphate; (d)IMP, (deoxy)inosine monophosphate; (d)XMP, (deoxy)xanthosine monophosphate; IMPDH, inosine monophosphate dehydrogenase; XMPP, xanthosine monophosphate phosphatase.

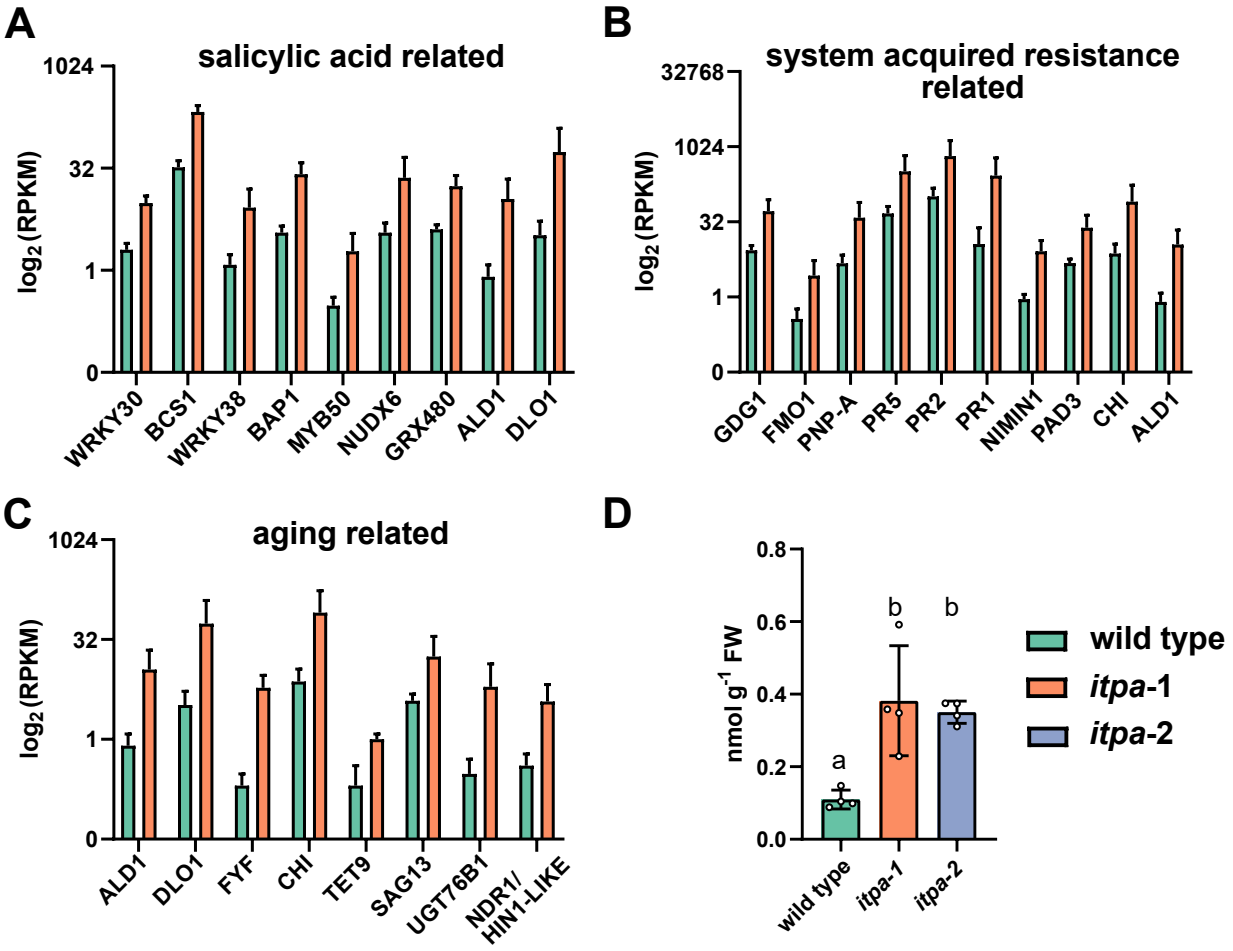

Figure 13. Loss-of-function of ITPA leads to differential upregulation of transcripts associated with salicylic acid, systemic acquired resistance as well as aging and increased endogenous concentrations of salicylic acid.

(A) RNA was isolated from 35-day-old Arabidopsis rosettes and analyzed by RNAseq. Log_2 (RPKM) values are shown for genes associated with response to salicylic acid (GO:0009751) and differentially regulated between wild type and *itpa-1* samples. Error bars are SD, $n = 3$. Every replicate represents a pool of two different plants. (B) As in (A) but for genes associated with systemic acquired resistance (GO:0009627). (C) As in (A) but for genes associated with aging (GO:0007568). (D) Concentrations of salicylic acid in 35-day-old Arabidopsis rosettes analyzed by LC-MS. Error bars are SD, $n = 4$. Every replicate represents a different plant. Statistical analysis was performed by a two-sided Tukey's pairwise comparison using the sandwich variance estimator. Different letters indicate p values < 0.05. All p values can be found in the Supplemental Table 1.

Parsed Citations

Abolhassani, N., Iyama, T., Tsuchimoto, D., Sakumi, K., Ohno, M., Behmanesh, M., and Nakabeppu, Y. (2010). NUDT16 and ITPA play a dual protective role in maintaining chromosome stability and cell growth by eliminating dIDP/IDP and dITP/ITP from nucleotide pools in mammals. Nucleic Acids Research 38 (9): 2891–2903.
Google Scholar: Author Only Title Only Author and Title

Aliaga-Franco, N., Zhang, C., Presa, S., Srivastava, A.K., Granell, A., Alabadí, D., Sadanandom, A., Blázquez, M.A., and Minguet, E.G. (2019). Identification of transgene-free CRISPR-edited plants of rice, tomato, and arabidopsis by monitoring DsRED fluorescence in dry seeds. Frontiers in Plant Science 10: 1150.
Google Scholar: Author Only Title Only Author and Title

Alonso, J.M., Stepanova, A.N., Leisse, T.J., Kim, C.J., Chen, H., Shinn, P., Stevenson, D.K., Zimmerman, J., Barajas, P., Cheuk, R., Gadrinab, C., Heller, C., Jeske, A., Koesema, E., Meyers, C.C., Parker, H., Prednis, L., Ansari, Y., Choy, N., Deen, H., Geralt, M., Hazari, N., Hom, E., Karnes, M., Mulholland, C., Ndubaku, R., Schmidt, I., Guzman, P., Aguilar-Henonin, L., Schmid, M., Weigel, D., Carter, D.E., Marchand, T., Risseeuw, E., Brogden, D., Zeko, A., Crosby, W.L., Berry, C.C., and Ecker, J.R. (2003). Genome-wide insertional mutagenesis of Arabidopsis thaliana. Science 301 (5633): 653–657.
Google Scholar: Author Only Title Only Author and Title

Andrews, S. (2010). FastQC: A Quality Control Tool for High Throughput Sequence Data. Available online at: http://www.bioinformatics.babraham.ac.uk/projects/fastqc/
Google Scholar: Author Only Title Only Author and Title

Baccolini, C., and Witte, C.-P. (2019). AMP and GMP catabolism in arabidopsis converge on xanthosine, which is degraded by a nucleoside hydrolase heterocomplex. The Plant Cell 31 (3): 734–751.
Google Scholar: Author Only Title Only Author and Title

Batista-Silva, W., Heinemann, B., Rugen, N., Nunes-Nesi, A., Araújo, W.L., Braun, H.-P., and Hildebrandt, T.M. (2019). The role of amino acid metabolism during abiotic stress release. Plant, Cell & Environment 42 (5): 1630–1644.
Google Scholar: Author Only Title Only Author and Title

Behmanesh, M., Sakumi, K., Abolhassani, N., Toyokuni, S., Oka, S., Ohnishi, Y.N., Tsuchimoto, D., and Nakabeppu, Y. (2009). ITPase-deficient mice show growth retardation and die before weaning. Cell death and differentiation 16 (10): 1315–1322.
Google Scholar: Author Only Title Only Author and Title

Braun, H.-P. (2020). The oxidative phosphorylation system of the mitochondria in plants. Mitochondrion 53: 66–75.
Google Scholar: Author Only Title Only Author and Title

Budke, B., and Kuzminov, A. (2006). Hypoxanthine incorporation is nonmutagenic in Escherichia coli. Journal of Bacteriology 188 (18): 6553–6560.
Google Scholar: Author Only Title Only Author and Title

Budke, B., and Kuzminov, A. (2010). Production of clastogenic DNA precursors by the nucleotide metabolism in Escherichia coli. Molecular Microbiology 75 (1): 230–245.
Google Scholar: Author Only Title Only Author and Title

Burgis, N.E., Brucker, J.J., and Cunningham, R.P. (2003). Repair system for noncanonical purines in Escherichia coli. Journal of Bacteriology 185 (10): 3101–3110.
Google Scholar: Author Only Title Only Author and Title

Burton, K., White, H., and Sleep, J. (2005). Kinetics of muscle contraction and actomyosin NTP hydrolysis from rabbit using a series of metal-nucleotide substrates. The Journal of Physiology 563 (Pt 3): 689–711.
Google Scholar: Author Only Title Only Author and Title

Cadet, J., and Wagner, J.R. (2013). DNA base damage by reactive oxygen species, oxidizing agents, and UV radiation. Perspectives in Biology 5 (2).
Google Scholar: Author Only Title Only Author and Title

Cao, Y., Tanaka, K., Nguyen, C.T., and Stacey, G. (2014). Extracellular ATP is a central signaling molecule in plant stress responses. Current Opinion in Plant Biology 20: 82–87.
Google Scholar: Author Only Title Only Author and Title

Carnelli, A., Michelis, M.I. de, and Rasi-Caldogno, F. (1992). Plasma Membrane Ca-ATPase of Radish Seedlings I. Biochemical characterization using ITP as a substrate. Plant Physiology 98 (3): 1196–1201.
Google Scholar: Author Only Title Only Author and Title

Carole L Linster, Emile Van Schaftingen, and Andrew D Hanson (2013). Metabolite damage and its repair or pre-emption. Nature Chemical Biology 9 (2): 72–80.
Google Scholar: Author Only Title Only Author and Title

Chen, M., Urs, M.J., Sánchez-González, I., Olayioye, M.A., Herde, M., and Witte, C.-P. (2018). m6A RNA degradation products are catabolized by an evolutionarily conserved N6-Methyl-AMP deaminase in plant and mammalian cells. The Plant Cell 30 (7): 1511–1522.
Google Scholar: Author Only Title Only Author and Title

Chen, M., and Witte, C.-P. (2020). A kinase and a glycosylase catabolize pseudouridine in the peroxisome to prevent toxic pseudouridine monophosphate accumulation. The Plant Cell 32 (3): 722–739.
Google Scholar: Author Only Title Only Author and Title

Cho, U.-H., and Seo, N.-H. (2005). Oxidative stress in Arabidopsis thaliana exposed to cadmium is due to hydrogen peroxide accumulation. Plant Science 168 (1): 113–120.
Google Scholar: Author Only Title Only Author and Title

Claus-Peter Witte, Laurent Noël, Janine Gielbert, Jane Parker, and Tina Romeis (2004). Rapid one-step protein purification from plant material using the eight-amino acid StrepII epitope. Plant Molecular Biology 55 (1): 135–147.
Google Scholar: Author Only Title Only Author and Title

Clough, S.J., and Bent, A.F. (1998). Floral dip: a simplified method for Agrobacterium-mediated transformation of Arabidopsis thaliana. The Plant Journal for Cell and Molecular Biology 16 (6): 735–743.
Google Scholar: Author Only Title Only Author and Title

Clyman, J., and Cunningham, R.P. (1987). Escherichia coli K-12 mutants in which viability is dependent on recA function. Journal of Bacteriology 169 (9): 4203–4210.
Google Scholar: Author Only Title Only Author and Title

Corpas, F.J., Leterrier, M., Valderrama, R., Airaki, M., Chaki, M., Palma, J.M., and Barroso, J.B. (2011). Nitric oxide imbalance provokes a nitrosative response in plants under abiotic stress. Plant Science 181 (5): 604–611.
Google Scholar: Author Only Title Only Author and Title

Crécy-Lagard, V. de, Haas, D., and Hanson, A.D. (2018). Newly-discovered enzymes that function in metabolite damage-control. Current Opinion in Chemical Biology 47: 101–108.
Google Scholar: Author Only Title Only Author and Title

Dahncke, K., and Witte, C.-P. (2013). Plant purine nucleoside catabolism employs a guanosine deaminase required for the generation of xanthosine in Arabidopsis. The Plant Cell 25 (10): 4101–4109.
Google Scholar: Author Only Title Only Author and Title

Davies, O., Mendes, P., Smallbone, K., and Malys, N. (2012). Characterisation of multiple substrate-specific (d)ITP/(d)XTPase and modelling of deaminated purine nucleotide metabolism. BMB Reports 45 (4): 259–264.
Google Scholar: Author Only Title Only Author and Title

Demidchik, V. (2015). Mechanisms of oxidative stress in plants: From classical chemistry to cell biology. Environmental and Experimental Botany 109: 212–228.
Google Scholar: Author Only Title Only Author and Title

DeVito, S., Woodrick, J., Song, L., and Roy, R. (2017). Mutagenic potential of hypoxanthine in live human cells. Mutation Research 803-805: 9–16.
Google Scholar: Author Only Title Only Author and Title

Di Sanità Toppi, L., and Gabbrielli, R. (1999). Response to cadmium in higher plants. Environmental and Experimental Botany 41 (2): 105–130.
Google Scholar: Author Only Title Only Author and Title

Dobrzanska, M., Szurmak, B., Wyslouch-Cieszynska, A., and Kraszewska, E. (2002). Cloning and characterization of the first member of the Nudix family from Arabidopsis thaliana. Journal of Biological Chemistry 277 (52): 50482–50486.
Google Scholar: Author Only Title Only Author and Title

Dubois, E., Córdoba-Cañero, D., Massot, S., Siaud, N., Gakière, B., Domenichini, S., Guérard, F., Roldan-Arjona, T., and Doutriaux, M.-P. (2011). Homologous recombination is stimulated by a decrease in dUTPase in Arabidopsis. PLoS ONE 6 (4): e18658.
Google Scholar: Author Only Title Only Author and Title

Fernie, A., Hashida, S.-N., Yoshimura, K., Gakière, B., Mou, Z., and Pétriacq, P. (2020). Editorial: NAD Metabolism and Signaling in Plants. Frontiers in Plant Science 11: 146.
Google Scholar: Author Only Title Only Author and Title

Fraser, J.H., Meyers, H., Henderson, J.F., Brox, L.W., and McCoy, E.E. (1975). Individual variation in inosine triphosphate accumulation in human erythrocytes. Clinical Biochemistry 8 (1-6): 353–364.
Google Scholar: Author Only Title Only Author and Title

Frederico, L.A., Kunkel, T.A., and Shaw, B.R. (1990). A sensitive genetic assay for the detection of cytosine deamination:

determination of rate constants and the activation energy. Biochemistry 29 (10): 2532–2537.
Google Scholar: Author Only Title Only Author and Title

Gall, A.D., Gall, A., Moore, A.C., Aune, M.K., Heid, S., Mori, A., and Burgis, N.E. (2013). Analysis of human ITPase nucleobase specificity by site-directed mutagenesis. Biochimie 95 (9): 1711–1721.
Google Scholar: Author Only Title Only Author and Title

Hadwiger, L.A., and Tanaka, K. (2017). Non-host resistance: DNA damage is associated with sa signaling for induction of pr genes and contributes to the growth suppression of a pea pathogen on pea endocarp tissue. Frontiers in Plant Science 8: 446.
Google Scholar: Author Only Title Only Author and Title

Haferkamp, I., Fernie, A.R., and Neuhaus, H.E. (2011). Adenine nucleotide transport in plants: much more than a mitochondrial issue. Trends in Plant Science 16 (9): 507–515.
Google Scholar: Author Only Title Only Author and Title

Handley, M.T., Reddy, K., Wills, J., Rosser, E., Kamath, A., Halachev, M., Falkous, G., Williams, D., Cox, P., Meynert, A., Raymond, E.S., Morrison, H., Brown, S., Allan, E., Aligianis, I., Jackson, A.P., Ramsahoye, B.H., Kriegsheim, A. von, Taylor, R.W., Finch, A.J., and FitzPatrick, D.R. (2019). ITPase deficiency causes a Martsolf-like syndrome with a lethal infantile dilated cardiomyopathy. PLoS Genetics 15 (3): e1007605.
Google Scholar: Author Only Title Only Author and Title

Hanson, A.D., Henry, C.S., Fiehn, O., and Crécy-Lagard, V. de (2016). Metabolite damage and metabolite damage control in plants. Annual Review of Plant Biology 67: 131–152.
Google Scholar: Author Only Title Only Author and Title

Harris, C., and Baulcombe, D. (2015). Chlorophyll content assay to quantify the level of necrosis induced by different R gene/elicitor combinations after transient expression. Bio-Protocol 5 (23).
Google Scholar: Author Only Title Only Author and Title

Heinemann, K.J., Yang, S.-Y., Straube, H., Medina-Escobar, N., Varbanova-Herde, M., Herde, M., Rhee, S., and Witte, C.-P. (2021). Initiation of cytosolic plant purine nucleotide catabolism involves a monospecific xanthosine monophosphate phosphatase. Nature communications 12 (1): 6846.
Google Scholar: Author Only Title Only Author and Title

Herberich, E., Sikorski, J., and Hothorn, T. (2010). A robust procedure for comparing multiple means under heteroscedasticity in unbalanced designs. PLoS ONE 5 (3): e9788.
Google Scholar: Author Only Title Only Author and Title

Holmes, S.L., Turner, B.M., and Hirschhorn, K. (1979). Human inosine triphosphatase: Catalytic properties and population studies. Clinica Chimica Acta 97 (2-3): 143–153.
Google Scholar: Author Only Title Only Author and Title

Hooper, C.M., Castleden, I.R., Tanz, S.K., Aryamanesh, N., and Millar, A.H. (2017). SUBA4: the interactive data analysis centre for Arabidopsis subcellular protein locations. Nucleic Acids Research 45 (D1): D1064-D1074.
Google Scholar: Author Only Title Only Author and Title

James, A.M., Seal, S.E., Bailey, A.M., and Foster, G.D. (2021). Viral inosine triphosphatase: A mysterious enzyme with typical activity, but an atypical function. Molecular Plant Pathology 22 (3): 382–389.
Google Scholar: Author Only Title Only Author and Title

Janků, M., Luhová, L., and Petřivalský, M. (2019). On the origin and fate of reactive oxygen species in plant cell compartments. Antioxidants (Basel, Switzerland) 8 (4).
Google Scholar: Author Only Title Only Author and Title

Ji, D., Stepchenkova, E.I., Cui, J., Menezes, M.R., Pavlov, Y.I., and Kool, E.T. (2017). Measuring deaminated nucleotide surveillance enzyme ITPA activity with an ATP-releasing nucleotide chimera. Nucleic Acids Research 45 (20): 11515–11524.
Google Scholar: Author Only Title Only Author and Title

Jiang, H.-P., Xiong, J., Liu, F.-L., Ma, C.-J., Tang, X.-L., Yuan, B.-F., and Feng, Y.-Q. (2018). Modified nucleoside triphosphates exist in mammals. Chemical Science 9 (17): 4160–4167.
Google Scholar: Author Only Title Only Author and Title

Kamiya, H. (2003). Mutagenic potentials of damaged nucleic acids produced by reactive oxygen/nitrogen species: approaches using synthetic oligonucleotides and nucleotides: survey and summary. Nucleic Acids Research 31 (2): 517–531.
Google Scholar: Author Only Title Only Author and Title

Keya, C.A., Crozier, A., and Ashihara, H. (2003). Inhibition of caffeine biosynthesis in tea (Camellia sinensis) and coffee (Coffea arabica) plants by ribavirin. FEBS Letters 554 (3): 473–477.
Google Scholar: Author Only Title Only Author and Title

Klinker, J.F., and Seifert, R. (1997). Functionally nonequivalent interactions of guanosine 5′-triphosphate, inosine 5′-triphosphate, and xanthosine 5′-triphosphate with the retinal G-protein, transducin, and with Gi-proteins in HL-60 leukemia cell membranes. Biochemical Pharmacology 54 (5): 551–562.
Google Scholar: Author Only Title Only Author and Title

Kong, R.P.W., Siu, S.O., Lee, S.S.M., Lo, C., and Chu, I.K. (2011). Development of online high-/low-pH reversed-phase-reversed-phase two-dimensional liquid chromatography for shotgun proteomics: a reversed-phase-strong cation exchange-reversed-phase approach. Journal of Chromatography. A 1218 (23): 3681–3688.
Google Scholar: Author Only Title Only Author and Title

Kumar, S., Stecher, G., Li, M., Knyaz, C., and Tamura, K. (2018). MEGA X: Molecular evolutionary genetics analysis across computing platforms. Molecular Biology and Evolution 35 (6): 1547–1549.
Google Scholar: Author Only Title Only Author and Title

Kuskovsky, R., Buj, R., Xu, P., Hofbauer, S., Doan, M.T., Jiang, H., Bostwick, A., Mesaros, C., Aird, K.M., and Snyder, N.W. (2019). Simultaneous isotope dilution quantification and metabolic tracing of deoxyribonucleotides by liquid chromatography high resolution mass spectrometry. Analytical Biochemistry 568: 65–72.
Google Scholar: Author Only Title Only Author and Title

Leiva, A.M., Jimenez, J., Sandoval, H., Perez, S., and Cuellar, W.J. (2022). Complete genome sequence of a novel secovirid infecting cassava in the Americas. Archives of Virology.
Google Scholar: Author Only Title Only Author and Title

Lerma-Ortiz, C., Jeffryes, J.G., Cooper, A.J.L., Niehaus, T.D., Thamm, A.M.K., Frelin, O., Aunins, T., Fiehn, O., Crécy-Lagard, V. de, Henry, C.S., and Hanson, A.D. (2016). 'Nothing of chemistry disappears in biology': the Top 30 damage-prone endogenous metabolites. Biochemical Society Transactions 44 (3): 961–971.
Google Scholar: Author Only Title Only Author and Title

Li, Z., Kim, J.H., Kim, J., Lyu, J.I., Zhang, Y., Guo, H., Nam, H.G., and Woo, H.R. (2020). ATM suppresses leaf senescence triggered by DNA double-strand break through epigenetic control of senescence-associated genes in Arabidopsis. The New Phytologist 227 (2): 473–484.
Google Scholar: Author Only Title Only Author and Title

Lin, S., McLennan, A.G., Ying, K., Wang, Z., Gu, S., Jin, H., Wu, C., Liu, W., Yuan, Y., Tang, R., Xie, Y., and Mao, Y. (2001). Cloning, expression, and characterization of a human inosine triphosphate pyrophosphatase encoded by the itpa gene. Journal of Biological Chemistry 276 (22): 18695–18701.
Google Scholar: Author Only Title Only Author and Title

Lin, A.-J., Zhang, X.-H., Chen, M.-M., and Cao, Q. (2007). Oxidative stress and DNA damages induced by cadmium accumulation. Journal of Environmental Sciences 19 (5): 596–602.
Google Scholar: Author Only Title Only Author and Title

Lindahl, T. (1993). Instability and decay of the primary structure of DNA. Nature 362 (6422): 709–715.
Google Scholar: Author Only Title Only Author and Title

Lindahl, T., and Nyberg, B. (1974). Heat-induced deamination of cytosine residues in deoxyribonucleic acid. Biochemistry 13 (16): 3405–3410.
Google Scholar: Author Only Title Only Author and Title

Littlejohn, G.R., Gouveia, J.D., Edner, C., Smirnoff, N., and Love, J. (2010). Perfluorodecalin enhances in vivo confocal microscopy resolution of Arabidopsis thaliana mesophyll. The New Phytologist 186 (4): 1018–1025.
Google Scholar: Author Only Title Only Author and Title

Liu, S., Yu, F., Yang, Z., Wang, T., Xiong, H., Chang, C., Yu, W., and Li, N. (2018). Establishment of Dimethyl Labeling-based Quantitative Acetylproteomics in Arabidopsis. Molecular & Cellular Proteomics 17 (5): 1010–1027.
Google Scholar: Author Only Title Only Author and Title

Lu, S., Wang, J., Chitsaz, F., Derbyshire, M.K., Geer, R.C., Gonzales, N.R., Gwadz, M., Hurwitz, D.I., Marchler, G.H., Song, J.S., Thanki, N., Yamashita, R.A., Yang, M., Zhang, D., Zheng, C., Lanczycki, C.J., and Marchler-Bauer, A. (2020). CDD/SPARCLE: the conserved domain database in 2020. Nucleic Acids Research 48 (D1): D265-D268.
Google Scholar: Author Only Title Only Author and Title

Galperin, M. Y., Moroz, O. V., Wilson, K. S., and Murzin, A. G. (2006). House cleaning, a part of good housekeeping. Molecular Microbiology 59 (1): 5–19.
Google Scholar: Author Only Title Only Author and Title

Muraoka, M., Fukuzawa, H., Nishida, A., Okano, K., Tsuchihara, T., Shimoda, A., Suzuki, Y., Sato, M., Osumi, M., and Sakai, H. (1999). The effects of various GTP analogues on microtubule assembly. Cell Structure and Function 24 (2): 101–109.
Google Scholar: Author Only Title Only Author and Title

Myrach, T., Zhu, A., and Witte, C.-P. (2017). The assembly of the plant urease activation complex and the essential role of the urease accessory protein G (UreG) in delivery of nickel to urease. The Journal of Biological Chemistry 292 (35): 14556–14565.
Google Scholar: Author Only Title Only Author and Title

Nagy, G.N., Leveles, I., and Vértessy, B.G. (2014). Preventive DNA repair by sanitizing the cellular (deoxy)nucleoside triphosphate pool. The FEBS journal 281 (18): 4207–4223.
Google Scholar: Author Only Title Only Author and Title

Niehaus, M., Straube, H., Künzler, P., Rugen, N., Hegermann, J., Giavalisco, P., Eubel, H., Witte, C.-P., and Herde, M. (2020). Rapid Affinity Purification of Tagged Plant Mitochondria (Mito-AP) for Metabolome and Proteome Analyses. Plant Physiology 182 (3): 1194–1210.
Google Scholar: Author Only Title Only Author and Title

Niehaus, T.D., Patterson, J.A., Alexander, D.C., Folz, J.S., Pyc, M., MacTavish, B.S., Bruner, S.D., Mullen, R.T., Fiehn, O., and Hanson, A.D. (2019). The metabolite repair enzyme Nit1 is a dual-targeted amidase that disposes of damaged glutathione in Arabidopsis. The Biochemical Journal 476 (4): 683–697.
Google Scholar: Author Only Title Only Author and Title

Niehaus, T.D., Richardson, L.G.L., Gidda, S.K., ElBadawi-Sidhu, M., Meissen, J.K., Mullen, R.T., Fiehn, O., and Hanson, A.D. (2014). Plants utilize a highly conserved system for repair of NADH and NADPH hydrates. Plant Physiology 165 (1): 52–61.
Google Scholar: Author Only Title Only Author and Title

Noskov, V.N., Staak, K., Shcherbakova, P.V., Kozmin, S.G., Negishi, K., Ono, B.-C., Hayatsu, H., and Pavlov, Y.I. (1996). HAM1, the gene controlling 6-N-hydroxylaminopurine sensitivity and mutagenesis in the yeast Saccharomyces cerevisiae. Yeast 12 (1): 17–29.
Google Scholar: Author Only Title Only Author and Title

Fernández-Bautista, N., Domínguez-Núñez, J. A., Moreno, M. M. C., and Berrocal-Lobo, M. (2016). Plant Tissue Trypan Blue Staining During Phytopathogen Infection. Bio-Protocol 6 (24): e2078-e2078.
Google Scholar: Author Only Title Only Author and Title

Oberacker, P., Stepper, P., Bond, D.M., Höhn, S., Focken, J., Meyer, V., Schelle, L., Sugrue, V.J., Jeunen, G.-J., Moser, T., Hore, S.R., Meyenn, F. von, Hipp, K., Hore, T.A., and Jurkowski, T.P. (2019). Bio-On-Magnetic-Beads (BOMB): Open platform for high-throughput nucleic acid extraction and manipulation. PLoS Biology 17 (1): e3000107.
Google Scholar: Author Only Title Only Author and Title

Osheroff, N., Shelton, E.R., and Brutlag, D.L. (1983). DNA topoisomerase II from Drosophila melanogaster. Relaxation of supercoiled DNA. Journal of Biological Chemistry 258 (15): 9536–9543.
Google Scholar: Author Only Title Only Author and Title

Pang, B., McFaline, J.L., Burgis, N.E., Dong, M., Taghizadeh, K., Sullivan, M.R., Elmquist, C.E., Cunningham, R.P., and Dedon, P.C. (2012). Defects in purine nucleotide metabolism lead to substantial incorporation of xanthine and hypoxanthine into DNA and RNA. Proceedings of the National Academy of Sciences of the United States of America 109 (7): 2319–2324.
Google Scholar: Author Only Title Only Author and Title

Pétriacq, P., Ton, J., Patrit, O., Tcherkez, G., and Gakière, B. (2016). NAD Acts as an Integral Regulator of Multiple Defense Layers. Plant Physiology 172 (3): 1465–1479.
Google Scholar: Author Only Title Only Author and Title

Pietrowska-Borek, M., Dobrogojski, J., Sobieszczuk-Nowicka, E., and Borek, S. (2020). New Insight into Plant Signaling: Extracellular ATP and Uncommon Nucleotides. Cells 9 (2).
Google Scholar: Author Only Title Only Author and Title

Rampazzo, C., Miazzi, C., Franzolin, E., Pontarin, G., Ferraro, P., Frangini, M., Reichard, P., and Bianchi, V. (2010). Regulation by degradation, a cellular defense against deoxyribonucleotide pool imbalances. Mutation Research 703 (1): 2–10.
Google Scholar: Author Only Title Only Author and Title

Rinne, J., Witte, C.-P., and Herde, M. (2021). Loss of MAR1 Function is a Marker for Co-Selection of CRISPR-Induced Mutations in Plants. Frontiers in Genome Editing 3: 723384.
Google Scholar: Author Only Title Only Author and Title

Rudd, S.G., Valerie, N.C.K., and Helleday, T. (2016). Pathways controlling dNTP pools to maintain genome stability. DNA Repair 44: 193–204.
Google Scholar: Author Only Title Only Author and Title

Sakumi, K., Abolhassani, N., Behmanesh, M., Iyama, T., Tsuchimoto, D., and Nakabeppu, Y. (2010). ITPA protein, an enzyme that eliminates deaminated purine nucleoside triphosphates in cells. Mutation Research 703 (1): 43–50.
Google Scholar: Author Only Title Only Author and Title

Savchenko, A., Proudfoot, M., Skarina, T., Singer, A., Litvinova, O., Sanishvili, R., Brown, G., Chirgadze, N., and Yakunin, A.F.

(2007). Molecular basis of the antimutagenic activity of the house-cleaning inosine triphosphate pyrophosphatase RdgB from Escherichia coli. Journal of Molecular Biology 374 (4): 1091–1103.
Google Scholar: Author Only Title Only Author and Title

Simone, P.D., Pavlov, Y.I., and Borgstahl, G.E.O. (2013). ITPA (inosine triphosphate pyrophosphatase): from surveillance of nucleotide pools to human disease and pharmacogenetics. Mutation Research 753 (2): 131–146.
Google Scholar: Author Only Title Only Author and Title

Spee, J.H., Vos, W.M. de, and Kuipers, O.P. (1993). Efficient random mutagenesis method with adjustable mutation frequency by use of PCR and dITP. Nucleic Acids Research 21 (3): 777–778.
Google Scholar: Author Only Title Only Author and Title

Stenmark, P., Kursula, P., Flodin, S., Gräslund, S., Landry, R., Nordlund, P., and Schüler, H. (2007). Crystal structure of human inosine triphosphatase. Substrate binding and implication of the inosine triphosphatase deficiency mutation P32T. Journal of Biological Chemistry 282 (5): 3182–3187.
Google Scholar: Author Only Title Only Author and Title

Straube, H., Niehaus, M., Zwittian, S., Witte, C.-P., and Herde, M. (2020). Enhanced nucleotide analysis enables the quantification of deoxynucleotides in plants and algae revealing connections between nucleoside and deoxynucleoside metabolism. The Plant Cell.
Google Scholar: Author Only Title Only Author and Title

Thomas, M.J., Platas, A.A., and Hawley, D.K. (1998). Transcriptional Fidelity and Proofreading by RNA Polymerase II. Cell 93 (4): 627–637.
Google Scholar: Author Only Title Only Author and Title

Tian, T., Liu, Y., Yan, H., You, Q., Yi, X., Du, Z., Xu, W., and Su, Z. (2017). agriGO v2.0: a GO analysis toolkit for the agricultural community, 2017 update. Nucleic Acids Research 45 (W1): W122-W129.
Google Scholar: Author Only Title Only Author and Title

Tomlinson, K.R., Pablo-Rodriguez, J.L., Bunawan, H., Nanyiti, S., Green, P., Miller, J., Alicai, T., Seal, S.E., Bailey, A.M., and Foster, G.D. (2019). Cassava brown streak virus Ham1 protein hydrolyses mutagenic nucleotides and is a necrosis determinant. Molecular Plant Pathology 20 (8): 1080–1092.
Google Scholar: Author Only Title Only Author and Title

Traube, F. R., Schiffers, S., Iwan, K., Kellner, S., Spada, F., Müller, M., and Carell, T. (2019). Isotope-dilution mass spectrometry for exact quantification of noncanonical DNA nucleosides. Nature Protocols 14 (1): 283–312.
Google Scholar: Author Only Title Only Author and Title

Tripathi, D., Nam, A., Oldenburg, D.J., and Bendich, A.J. (2020). Reactive Oxygen Species, Antioxidant Agents, and DNA Damage in Developing Maize Mitochondria and Plastids. Frontiers in Plant Science 11: 596.
Google Scholar: Author Only Title Only Author and Title

Valderrama, R., Corpas, F.J., Carreras, A., Fernández-Ocaña, A., Chaki, M., Luque, F., Gómez-Rodríguez, M.V., Colmenero-Varea, P., Del Río, L.A., and Barroso, J.B. (2007). Nitrosative stress in plants. FEBS Letters 581 (3): 453–461.
Google Scholar: Author Only Title Only Author and Title

Vanderheiden, B.S. (1969). Genetic studies of human erythrocyte inosine triphosphatase. Biochemical Genetics 3 (3): 289–297.
Google Scholar: Author Only Title Only Author and Title

Vanderheiden, B.S. (1979). Possible implication of an inosinetriphosphate metabolic error and glutamic acid decarboxylase in paranoid schizophrenia. Biochemical Medicine 21 (1): 22–32.
Google Scholar: Author Only Title Only Author and Title

Wang, C., and Liu, Z. (2006). Arabidopsis ribonucleotide reductases are critical for cell cycle progression, DNA damage repair, and plant development. The Plant Cell 18 (2): 350–365.
Google Scholar: Author Only Title Only Author and Title

Wang, Z.-P., Xing, H.-L., Dong, L., Zhang, H.-Y., Han, C.-Y., Wang, X.-C., and Chen, Q.-J. (2015). Egg cell-specific promoter-controlled CRISPR/Cas9 efficiently generates homozygous mutants for multiple target genes in Arabidopsis in a single generation. Genome Biology 16: 144.
Google Scholar: Author Only Title Only Author and Title

Weber, J., and Senior, A.E. (2001). Bi-site catalysis in F1-ATPase: does it exist? Journal of Biological Chemistry 276 (38): 35422–35428.
Google Scholar: Author Only Title Only Author and Title

Witte, C.-P., and Herde, M. (2020). Nucleotide Metabolism in Plants. Plant Physiology 182 (1): 63–78.
Google Scholar: Author Only Title Only Author and Title

Witte, C.-P., Rosso, M.G., and Romeis, T. (2005). Identification of three urease accessory proteins that are required for urease activation in Arabidopsis. Plant Physiology 139 (3): 1155–1162.
Google Scholar: Author Only Title Only Author and Title

Yan, S., Wang, W., Marqués, J., Mohan, R., Saleh, A., Durrant, W.E., Song, J., and Dong, X. (2013). Salicylic acid activates DNA damage responses to potentiate plant immunity. Molecular Cell 52 (4): 602–610.
Google Scholar: Author Only Title Only Author and Title

Yang, Z.-B., He, C., Ma, Y., Herde, M., and Ding, Z. (2017). Jasmonic Acid Enhances Al-Induced Root Growth Inhibition. Plant Physiology 173 (2): 1420–1433.
Google Scholar: Author Only Title Only Author and Title

Yoneshima, Y., Abolhassani, N., Iyama, T., Sakumi, K., Shiomi, N., Mori, M., Shiomi, T., Noda, T., Tsuchimoto, D., and Nakabeppu, Y. (2016). Deoxyinosine triphosphate induces MLH1/PMS2- and p53-dependent cell growth arrest and DNA instability in mammalian cells. Scientific Reports 6: 32849.
Google Scholar: Author Only Title Only Author and Title

Yoshimura, K., Ogawa, T., Ueda, Y., and Shigeoka, S. (2007). AtNUDX1, an 8-oxo-7,8-dihydro-2'-deoxyguanosine 5'-triphosphate pyrophosphohydrolase, is responsible for eliminating oxidized nucleotides in Arabidopsis. Plant & Cell Physiology 48 (10): 1438–1449.
Google Scholar: Author Only Title Only Author and Title

Yu, D., Song, W., Tan, E.Y.J., Liu, L., Cao, Y., Jirschitzka, J., Li, E., Logemann, E., Xu, C., Huang, S., Jia, A., Chang, X., Han, Z., Wu, B., Schulze-Lefert, P., and Chai, J. (2021). TIR domains of plant immune receptors are 2′,3′-cAMP/cGMP synthetases mediating cell death. bioRxiv
Google Scholar: Author Only Title Only Author and Title